Advanced Physical Research
Vol.7, No.1, 2025, pp.5-28
https://doi.org/10.62476/apr.7105

APPLICATION OF NANOSCALE BORON NITRIDE FOR ENCAPSULATION OF NOXIOUS TRANSITION METALS (Cr, Mn, Fe, Zn, W, Cd) IN SOIL: PHYSICO-CHEMICAL CHARACTERIZATION USING DFT MODELING

Fatemeh Mollaamin[1*], **Majid Monajjemi**[2]

[1]Department of Biomedical Engineering, Faculty of Engineering and Architecture, Kastamonu University, Kastamonu, Turkiye
[2]Department of Chemical Engineering, Central Tehran Branch, Islamic Azad University, Tehran, Iran

Abstract. Particular attention is paid to searching for the stable configurations, calculating the corresponding binding energies, and evaluating the encapsulation of TMs inside the bare B_5N_{10} based on the partial and total density of states (PDOS and TDOS), electron localization function (ELF), electronic and magnetic properties of nanoclusters. B_5N_{10} was designed in the existence of TM. Furthermore, the nuclear magnetic resonance (NMR) analysis indicated the notable peaks surrounding Cr, Mn, Fe, Zn, W, Cd through the trapping in the bare B_5N_{10} during atom detection and removal from soil; however, it can be seen some fluctuations in the chemical shielding treatment of isotropic and anisotropy tensors. The selectivity of toxic metal elements adsorption by bare B_5N_{10} have been indicated as: $Cd > Zn > Fe > Cr > Mn \approx W$. The interaction state between contaminants and BN-based compounds are surface complexation and electrostatic interactions. This research article is beneficial to further comprehend the interactions of contaminants with BN-based compounds, which is also helpful for the improvement of BN-based compounds and potential areas for future applications in environment treatment. The toxic metal elements–adsorbed might be applied to design and expand the optoelectronic specifications of BN-based materials for generating photoelectric instruments toward soil purification.

Keywords: Encapsulated transition metals, contaminated soil bare B_5N_{10}, density of state, DFT Modeling.
Corresponding author: Fatemeh Mollaamin, Department of Biomedical Engineering, Faculty of Engineering and Architecture, Kastamonu University, Kastamonu, Turkiye, e-mail: *fmollaamin@kastamonu.edu.tr*
Received: 19 October 2024; Revised: 1 January 2025; Accepted: 14 January 2025; Published: 20 February 2025.

1 Introduction

Contamination by metals can be indicated by the changes in chemical, biochemical, and microbial properties of soils and plant responses. The total concentration of toxic metals in soil is still the most widely used indicator for risk assessment although extractable amounts have been reported to be more closely related to plant uptake. Heavy metals remark to some metals and metalloids having biological toxicity like Cd, Hg, As, Pb, and Cr (Li et al., 2019). Heavy metal contamination to soil and the environment has been accelerated in modern society due to industrialization, rapidly expanded world population, and intensified agriculture. Accumulation

How to cite (APA): Mollaamin, F., Monajjemi, M. (2025). Application of nanoscale boron nitride for encapsulation of noxious transition metals (Cr, Mn, Fe, Zn, W, Cd) in soil: Physico-chemical characterization using DFT modeling. *Advanced Physical Research, 7*(1), 5-28 https://doi.org/10.62476/apr.7105

of heavy metals often results in soil/water degradation and ecosystem malfunction. Moreover, heavy metals enter food chains from polluted soil, water, and air, and consequently cause food contamination, thus posing a threat to human and animal health (Onawumi et al., 2024; Rahman et al., 2012; Thuy et al., 2000).

Trace metals in soils and dusts can be accumulated in the human body via direct inhalation, ingestion, and dermal contact absorption (De Miguel et al., 1998; Madrid et al., 2002; Meza-Montenegro et al., 2012; Sun et al., 2013) or via the soil-crop system (Liu et al., 2007; Sun et al., 2013). The anthropogenic sources of metals include traffic emission, industrial and domestic emission, atmospheric deposition, mining, waste disposal, sewage, pesticides, and fertilizers (Sezgin et al., 2003; Montagne et al., 2007; Li et al., 2008; Morton-Bermea et al., 2009). Without proper management, abandoned mines will cause more serious environmental impacts compared with active mines (Ji et al., 2013). Consumption of food crops growing in contaminated area is one of the important sources of human exposure to metals in mining areas (Liu et al., 2005; Kim et al., 2011; Kachenko & Singh, 2006).

Soil contamination in urban environment by trace metals is of public concerns. For better risk assessment, it is important to determine their background concentrations in urban soils. For instance, Molybdenum (Mo) is an essential trace element for human, animal, and plant health. Mo deficiency in soils has frequently been reported, especially under P-deficient conditions. However, Mo is also a potentially toxic contaminant to soils and aquifers that may pose significant threat to ecological and human health (Motuzova et al., 2014).

Another research studied the sources and extent of arsenic (As) contamination and the translocation and speciation from microbes to soil are illustrated (Al-Makishah et al., 2020). Moreover, several activities can build up soil copper (Cu) concentrations leading to incorporation into the food chain and adversely affect natural and managed ecosystems (Poggere et al., 2023). The cobalt (Co)-contaminated soil has exposed potential toxicity to humans, plants, and animals. Recently, scientists have summarized the natural and anthropogenic sources arousing the increase of cobalt in soil and review the cobalt species in soil and factors that influence the mobilization of cobalt (Jiang et al., 2022).

Soil contamination in urban environment by trace metals is of public concerns. For better risk assessment, it is important to determine their background concentrations in urban soils. One investigation determined the concentrations of 9 trace metals including As, Ba, Cd, Co, Cu, Ni, Pb, Se, and Zn in 214 urban soils from 6 cities of different sizes from both public and commercial sites in Florida (da Silva et al., 2010).

Boron nitride nanomaterials have been used owing to their unique characteristics such as eco-friendly attributes for pollutant adsorption, big surface area, high chemical & mechanical strength and semiconducting property (Mollaamin & Monajjemi, 2024a; Mishra & Saravanan, 2018; Weng et al., 2016; Mollaamin & Monajjemi, 2024b). Boron nitride nanometerials usually exhibit semi-leading behavior, which is considered a proper alternative to carbon nanotubes. The properties of boron and nitrogen atoms which are the first neighbors of carbon in the periodic table, make boron nitride an interesting subject of numerous studies (Shtansky et al., 2022; Mollaamin et al., 2024; Davies et al., 2018). In recent years, different investigations on the adsorption of chemical contaminants and applying various boron nitride nanomaterials as adsorbents for water purification have been studied (Mollaamin & Monajjemi, 2024c; Chao et al., 2020; Mollaamin, 2024). Various physical shapes of boron nitride (BN)-based nano adsorbents such as nanoparticles, fullerenes, nanotubes, nanofibers, nanoribbons, nanosheets, nanomeshes, nanoflowers, and hollow spheres have been broadly considered possible adsorbents owing to their exceptional characteristics such as large surface area, structural variability, great chemical/mechanical strength, abundant structural defects, high reactive sites, and functional groups (Mollaamin & Monajjemi, 2024d; Guo et al., 2029).

In this work, bare B_5N_{10} has been modeled for trapping TMs including Cr, Mn, Fe, Zn, W, Cd. Physical and chemical properties of the interaction binding between Cr, Mn, Fe, Zn, W, Cd,

and boron/ nitrogen in bare B_5N_{10} have been estimated. The encapsulated layer materials can act as sieves for atoms or molecules, and the functional groups on the surface of the encapsulated layer material can selectively complex with certain specific contaminants, thereby facilitating the selective contamination removal.

2 Nanomaterials and DFT method

2.1 Trapping metal elements in bare B_5N_{10}

The intention is to remove Cr, Mn, Fe, Zn, W, Cd from the soil medium containing toxic ingredients. The soil medium consists of metal atoms and the added bare B_5N_{10} (Figure 1). Bare B_5N_{10} was modeled in the presence of Cr, Mn, Fe, Zn, W, Cd through computational methods of density functional method of CAM–B3LYP–D3.

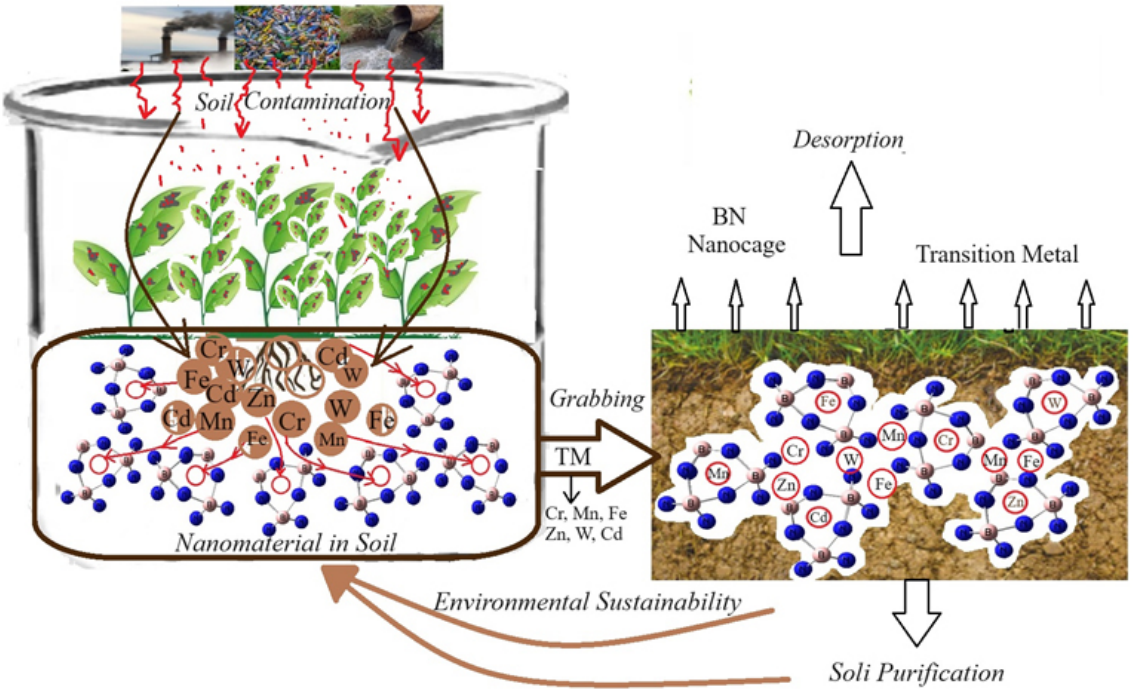

Figure 1: Trapping of some contaminant elements of Cr, Mn, Fe, Zn, W, Cd in polluted soil via B_5N_{10} and formation of $(a)Cr@B_5N_{10}$, $(b)Mn@B_5N_{10}$, $(c)Fe@B_5N_{10}$, $(d)Zn@B_5N_{10}$, $(e)W@B_5N_{10}$, and $(f)Cd@B_5N_{10}$ complexes toward clean soil

The metal atoms were successfully incorporated in the center of bare B_5N_{10} toward formation of $Cr@B_5N_{10}$, $Mn@B_5N_{10}$, $Fe@B_5N_{10}$, $Zn@B_5N_{10}$, $W@B_5N_{10}$, and $Cd@B_5N_{10}$ complexes (Figure1) and charge distribution of these complexes has been computed owing to the parameter of Bader charge evaluation (Henkelman et al., 2006). Irrespective of what element, the bare B_5N_{10} becomes bigger for embedding these elements.

2.2 Method of Density functional theory (DFT)

There are many ions and electrons in a metallic solid which form a many-body system. DFT has been performed in this article due to projector/ameliorated/wave method, Perdew/Burke/Ernzerhof functional based on the generalized gradient approximation as the exchange-correlation functional, and non-empirical PBE functional (Mollaamin & Monajjemi, 2024e; Perdew et al.,1996; Zadeh et al., 2015).

For years, metals and metalloids with computed bandwidths have been an important discussion through DFT (Ziesche et al., 1998). In this paper, the first principles calculations for

trapping TMs consisting of Cr, Mn, Fe, Zn, W, Cd by bare B_5N_{10} using DFT methods have been performed.

The electronic density within the Kohn-Sham (KS) equations leads us to a considerable reduction of quantum computing towards Hamiltonian parameter (Hohenberg & Kohn, 1964; Kohn & Sham, 1965):

$$\hat{H}_s = -\sum_i^M \frac{1}{2}\,\overrightarrow{\nabla}_i^2 + \sum_i^M v_s(\overrightarrow{r}_i) \;=\; \sum_i^M \hat{h}_s; \hat{h}_s = -\frac{1}{2}\,\overrightarrow{\nabla}_i^2 + v_s\,(\overrightarrow{r}_i) \tag{1}$$

where M is non-interactive electrons, v_s is external potential. Thus, by measuring ψ_i (single particle orbitals), the parameter of electronic densities for electrons with noninteractions will be:

$$\rho\,(\overrightarrow{r}) = \sum_i^M |\psi_i\;(\overrightarrow{r})|^2 \tag{2}$$

So, the total energy will be:

$$\begin{aligned} E[\rho] = \sum_i^M n_i \left\langle \psi_i \left| -\tfrac{1}{2}\bar{V}^2 + v_{ext}(\vec{r}) + \tfrac{1}{2}\tfrac{\rho(\vec{r}')}{|\vec{r}-\vec{r}'|} d\vec{r}' \right| \psi_i \right\rangle + \\ + E_{xc}[\rho] + \tfrac{1}{2}\sum_\beta^N \sum_{\alpha\neq\beta}^N \tfrac{z_\alpha z_\beta}{|\vec{R}_\alpha - \vec{R}_\beta|}. \end{aligned} \tag{3}$$

Furthermore, B3LYP (Becke, Lee, Yang, Parr) function as a hybrid functional of 3-parameter basis function and LANL2DZ basis set for metals and metalloids within DFT approach (Becke, 1993; Lee et al., 1988; Kim & Jordan, 1994; Stephens et al., 1994; Cramer, 2004; Vosko et al., 1980). In addition, a new hybrid exchange–correlation functional called CAM–B3LYP was suggested which merges B3LYP and the long-range correction (Yanai et al., 2004). Moreover, the DFT functionals with the Grimme's D3 correction has been considered (Grimme et al., 2010). The approach of dispersion correction is added to Kohn-Sham density functional theory (DFT-D) with higher accuracy (Grimme et al., 2011).

In this work, DFT computations was accomplished by Gaussian 16 revision C.01 program package (Frisch et al., 2016). The z-matrix coordination has been built for trapping TM containing Cr, Mn, Fe, Zn, W, Cd in soil by the bare B_5N_{10} using GaussView 6.1 (Dennington et al., 2016) via the solid model and coordination (Figure 2).

The consequences will remark on the following challenges faced by the DFT approaches in accurately describing the (TMs) - (boron and nitrogen) bonding.

3 Results and Discussions

Bare B_5N_{10} has been modeled for trapping TMs including Cr, Mn, Fe, Zn, W, Cd. Physical and chemical properties of the interaction binding between Cr, Mn, Fe, Zn, W, Cd, and boron/ nitrogen in bare B_5N_{10} have been estimated.

3.1 ELF analysis

type of scalar fields called electron localization function (ELF) may demonstrate a broad span of bonding samples. Nevertheless, the distinction between deduced/raised electron delocalization/localization into cyclic π-conjugated sets stays encouraging for ELF (Matta *et al.*, 2024). The grosser the electron localization is in an area, the more likely the electron movement is restricted within it. Therefore, they might be discerned from the ones away if electrons are totally centralized. As Bader investigated, the zones with large electron localization possess extensive magnitudes of Fermi hole integration (Bader, 2001). But, with having a six-dimension function

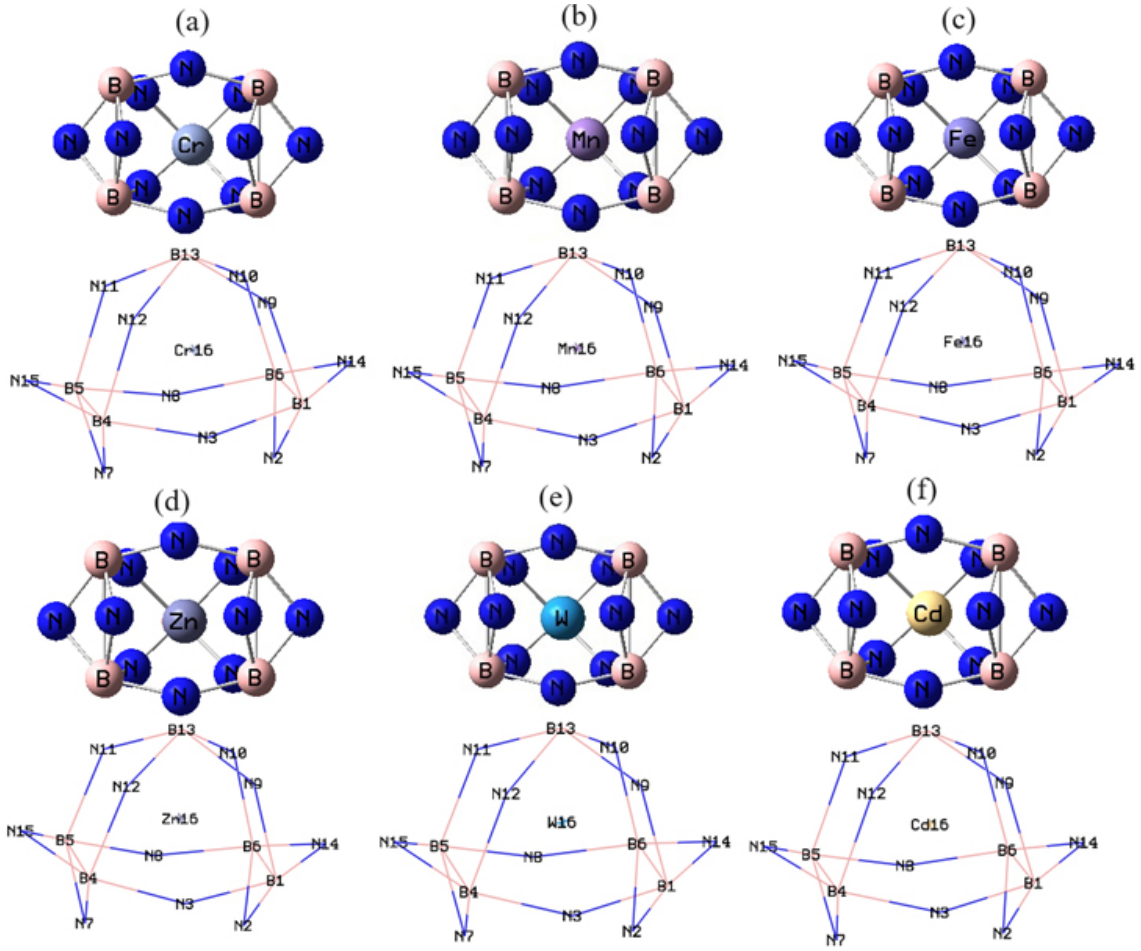

Figure 2: Optimized complexes of $(a)Cr@B_5N_{10}$, $(b)Mn@B_5N_{10}$, $(c)Fe@B_5N_{10}$, $(d)Zn@B_5N_{10}$, $(e)W@B_5N_{10}$, and $(f)Cd@B_5N_{10}$ using CAM–B3LYP–D3/EPR–3, LANL2DZ.

for the Fermi hole, it seems hard to be studied directly. Then, Becke and Edgecombe remarked that spherically averaged like spin conditional pair probability possesses a direct correlation with the Fermi hole and proposed the parameter of ELF in Multiwfn program (Lu & Chen, 2012; Lu, 2024) and popularized for spin-polarized procedure (Becke & Edgecombe,1990):

$$\mathrm{ELF}\,(\mathrm{r}) = \frac{1}{1 + [D(\mathrm{r})/D_0(\mathrm{r})]}, \tag{4}$$

where

$$D\,(\mathrm{r}) = \frac{1}{2}\sum_i \eta_i |\nabla\varphi_i\ (\mathrm{r})|^2 - \frac{1}{8}\left[\frac{|\nabla\rho_\alpha\ (\mathrm{r})|^2}{\rho_\alpha\ (\mathrm{r})} + \frac{|\nabla\rho_\beta\ (\mathrm{r})|^2}{\rho_\beta\ (\mathrm{r})}\right], \tag{5}$$

and

$$D_0\,(\mathrm{r}) = \frac{3}{10}\left(6\pi^2\right)^{2/3}\left[\rho_\alpha\ (\mathrm{r})^{5/3} + \rho_\beta\ (\mathrm{r})^{5/3}\right]. \tag{6}$$

For close-shell system, since $\rho_\alpha = \rho_\beta = (1/2)\,\rho$, D and $D0$ terms can be simplified as:

$$D\,(\mathrm{r}) = \frac{1}{2}\sum_i \eta_i |\nabla\varphi_i\ (\mathrm{r})|^2 - \frac{1}{8}\frac{|\nabla\rho\ (\mathrm{r})|^2}{\rho\ (\mathrm{r})}, \tag{7}$$

and

$$D_0\,(\mathrm{r}) = (3/10)\left(3\pi^2\right)^{2/3}\,\rho\;(\mathrm{r})^{5/3}. \tag{8}$$

Regarding kinetic energy, ELF was rechecked to be more punctual for both Kohn-Sham DFT and post-HF wavefunctions (Savin et al., 1992). In fact, the excess kinetic energy density caused by Pauli repulsion was unfolded by $D(r)$ and $D_0(r)$ may be inspected as Thomas-Fermi kinetic energy density. Because $D_0(r)$ is brough forward the ELF as origin, what the ELF shows is an affiliate localization. Encapsulation of TMs by bare B_5N_{10} towards formation of $Cr@B_5N_{10}$, $Mn@B_5N_{10}$, $Fe@B_5N_{10}$, $Zn@B_5N_{10}$, $W@B_5N$, and $Cd@B_5N_{10}$ nanoclusters can be defined by ELF graphs owing to exploring their delocalization/localization characterizations of electrons and chemical bonds (Figure 3a–f).

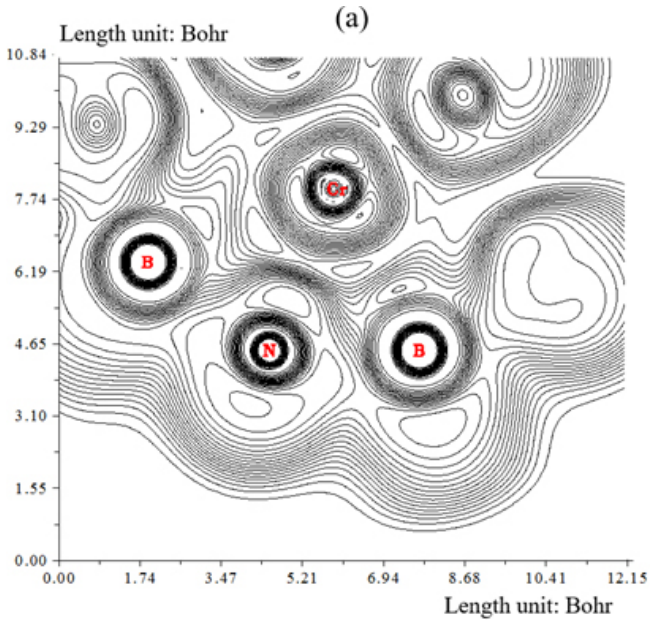

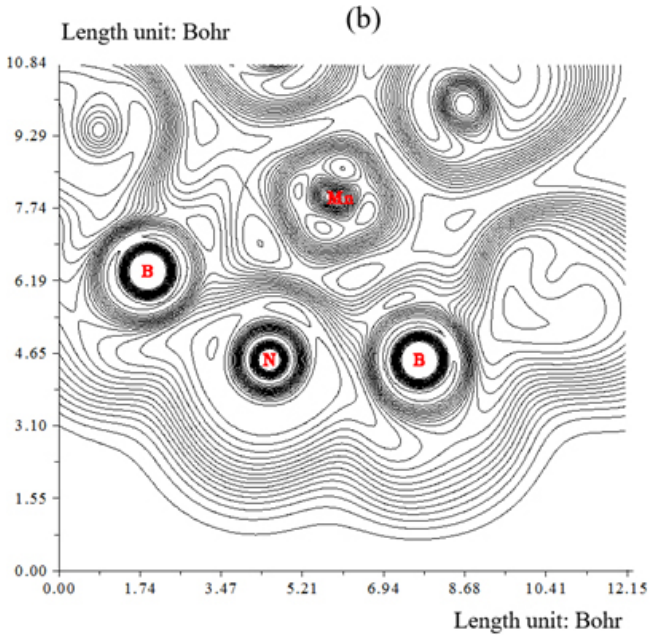

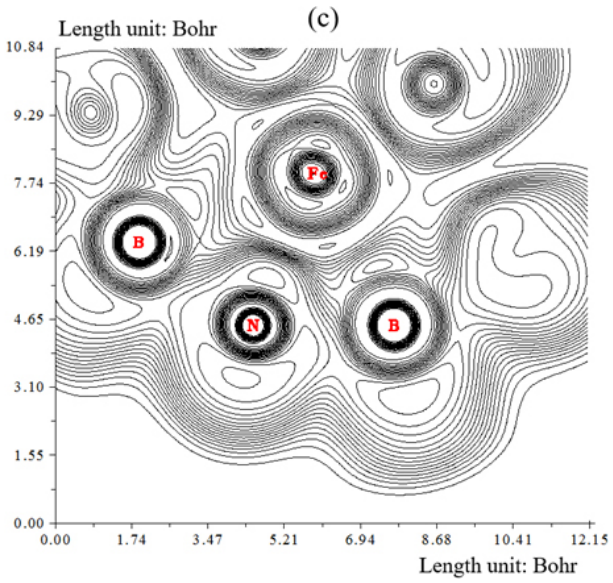
(c)
Length unit: Bohr
10.84
9.29
7.74
6.19
4.65
3.10
1.55
0.00
Fe
B
N
B
0.00
1.74
3.47
5.21
6.94
8.68
10.41
12.15
Length unit: Bohr

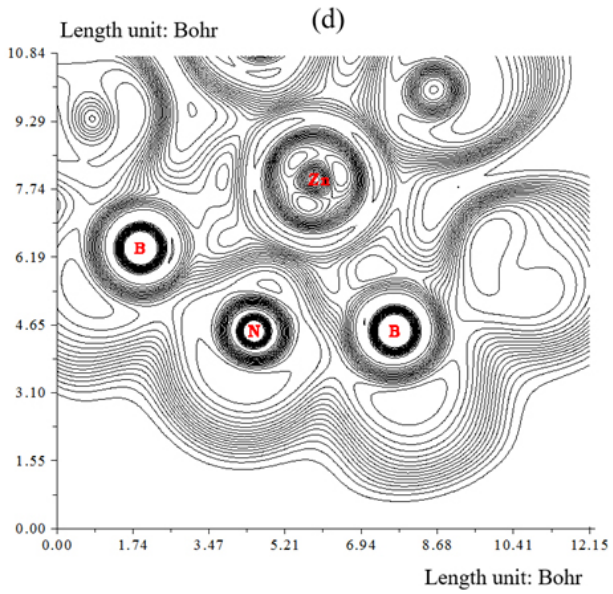
(d)
Length unit: Bohr
10.84
9.29
7.74
6.19
4.65
3.10
1.55
0.00
Zr
B
N
B
0.00
1.74
3.47
5.21
6.94
8.68
10.41
12.15
Length unit: Bohr

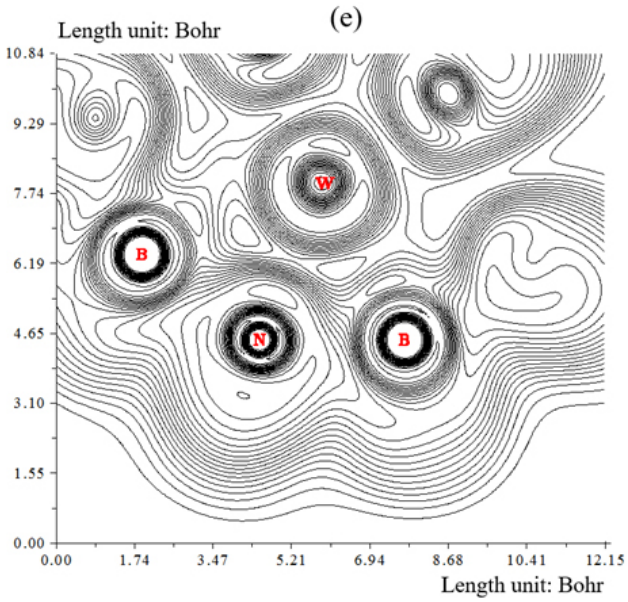
(e)
Length unit: Bohr
10.84
9.29
7.74
6.19
4.65
3.10
1.55
0.00
W
B
N
B
0.00
1.74
3.47
5.21
6.94
8.68
10.41
12.15
Length unit: Bohr

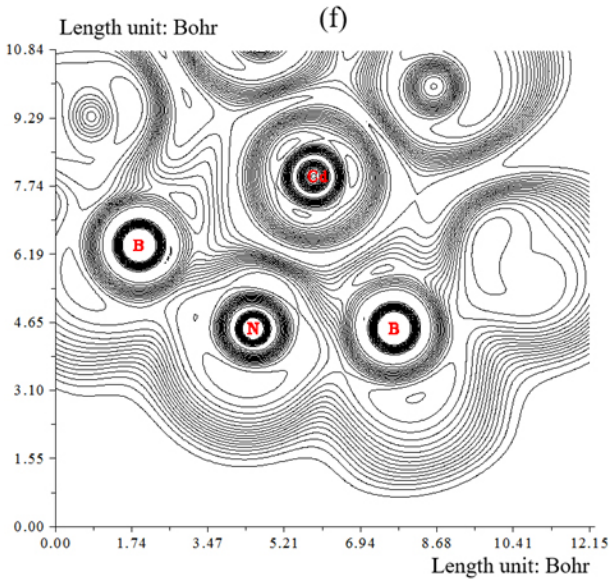

Figure 3: ELF graphs for TMs-encapsulated into bare B_5N_{10} towards formation of complexes including $(a)Cr@B_5N_{10}$, $(b)Mn@B_5N_{10}$, $(c)Fe@B_5N_{10}$, $(d)Zn@B_5N_{10}$, $(e)W@B_5N$, and $(f)Cd@B_5N_{10}$ by CAM–B3LYP–D3/6–311+G (d,p), LANL2DZ

A vaster jointed area engaged by an isosurface map has shown the electron delocalization in Cr@B_5N_{10}, Mn@B_5N_{10}, Fe@B_5N_{10}, Zn@B_5N_{10}, W@B_5N, and Cd@B_5N_{10} through labeling atoms of B1, N3, B4, N9, N12, B13, TM16 (TM=Cr, Mn, Fe, Zn, W, Cd). In fact, the counter map of ELF can confirm that bare B_5N_{10} can be efficient for TMs encapsulation towards formation of Cr@B_5N_{10}, Mn@B_5N_{10}, Fe@B_5N_{10}, Zn@B_5N_{10}, W@B_5N, and Cd@B_5N_{10} nanoclusters.

3.2 Density of states as TDOS and PDOS

Squirming the molecular orbital data owing to gaussian graphs of unit altitude and entire width at "half maximum (FWHM)" of 0.3 eV by "GaussSum 3.0.2" (O'Boyle et al., 2008) have computed total density of states (TDOS) diagrams. Regarding TM-encapsulated inside bare B_5N_{10} and the Cr@B_5N_{10}, Mn@B_5N_{10}, Fe@B_5N_{10}, Zn@B_5N_{10}, W@B_5N_{10}, and Cd@B_5N_{10} nanoclusters, TDOS has been measured. This parameter can indicate the existence of important chemical interactions often on the convex side (Figure 4a–f).

Figure 4 $(a' - f')$ shows the projected density of state (PDOS) of TMs@B_5N_{10} through Cr, Mn, Fe, Zn, W, Cd encapsulation. The existence of the energy states (p-orbital) of B, N, and (d-orbital) of Cr, Mn, Fe, Zn, W, Cd within the gap of TMs@B_5N_{10} induces the reactivity of the system. It is clear from the figure that after trapping of TMs, there is a significant contribution of d-orbital in the unoccupied level. Therefore, the curve of partial PDOS has described that p states of B, N atoms in B_5N_{10} and d-orbital of Cr, Mn, Fe, Zn, W, Cd in TMs@B_5N_{10} overcome due to the conduction band (Figure $4a' - f'$). A distinguished adsorption trait might be seen in TMs@B_5N_{10} because of the potent interaction between the p states of boron and nitrogen in B_5N_{10} with d states of Cr, Mn, Fe, Zn, W, Cd in TMs@B_5N_{10} complexes.

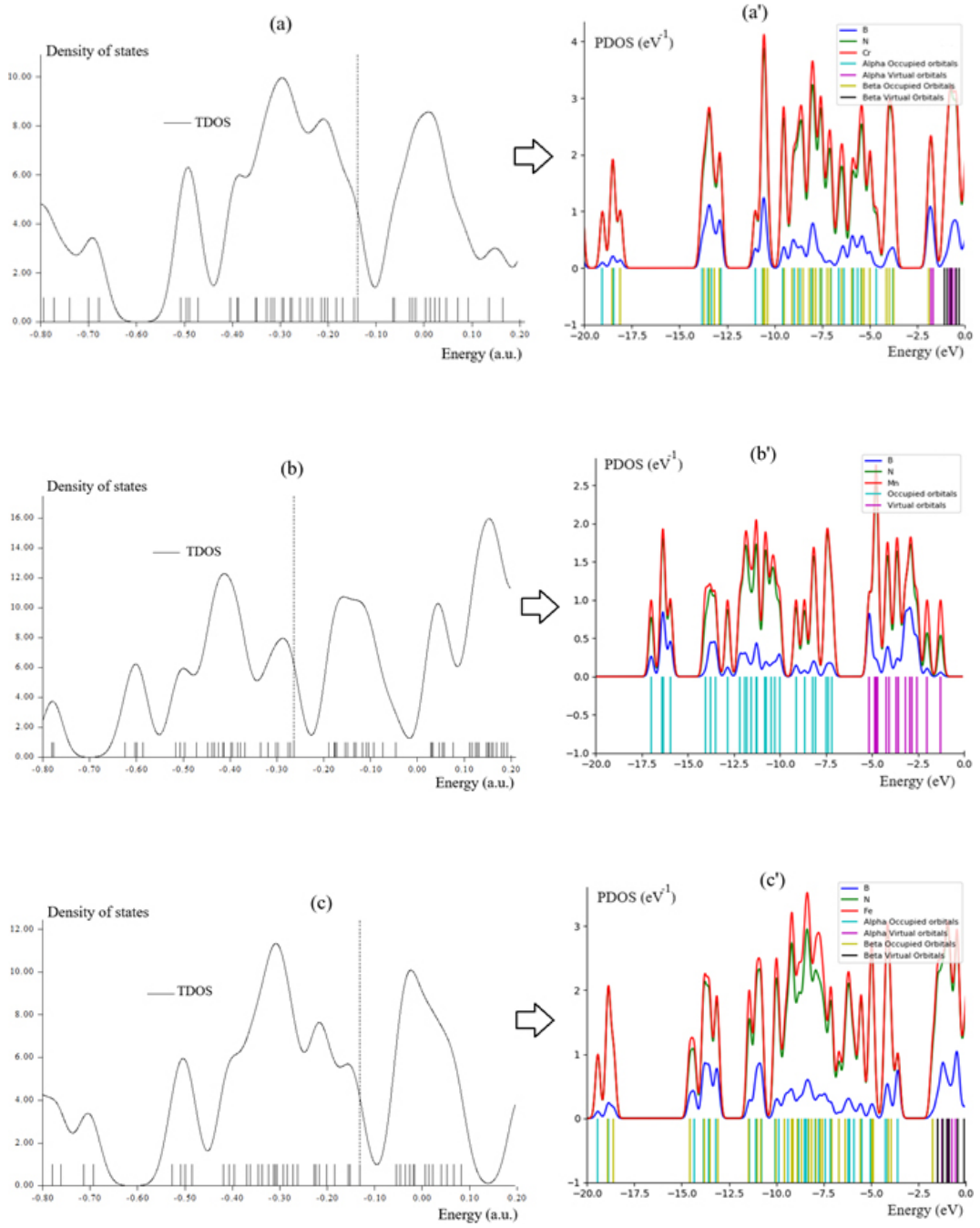

Figure 4: TDOD and PDOS graphs for TMs-encapsulated into bare B_5N_{10} towards formation of complexes including $a, a'-$ Cr@B_5N_{10}, $b, b'-$ Mn@B_5N_{10}, $c, c'-$ Fe@B_5N_{10}, $d, d'-$ Zn@B_5N_{10}, $e, e'-$ W@B_5N, and $f, f'-$ Cd@B_5N_{10}, respectively, by CAM–B3LYP–D3/6–311+G (d,p), LANL2DZ.

Figure 4($a' - f'$) shows that Cr@B_5N_{10}, Mn@B_5N_{10}, Fe@B_5N_{10}, Zn@B_5N_{10}, W@B_5N_{10}, and Cd@B_5N_{10} complexes have the most contribution at the middle of the conduction band between –5 to –15 eV, while contribution of boron and nitrogen states are enlarged and similar together, and grabbing of Cr, Mn, Fe, Zn, W, Cd depicts interfacial electronic of the bare B_5N_{10} for selection of these atoms. Cr @B_5N_{10} has indicated one sharp peak around –10 eV for Cr in Figure 4(a'), while Mn@B_5N_{10} (Figure 4b') has a sharp peak around –5 eV for Mn. The complexes of Fe@B_5N_{10} (Figure 4c') and Zn@B_5N_{10} (Figure 4d') have exhibited a sharp peak around –8.5 eV for Fe and Zn atoms, respectively. Furthermore, W@B_5N_{10} (Figure 4e') has exhibited a strong peak around –10 eV through the graphs for W. Moreover, Cd graph in Cd@B_5N_{10} (Figure 4f') with a sharp peak around –12.5 eV attracts our attention.

3.3 NQR towards nalysis of electric potential

In this work, the quantum mechanics of nuclear quadrupole resonance (NQR) at zero-field containing the magnitudes of nuclear quadrupole moments have been carried out on trapping Cr, Mn, Fe, Zn, W, Cd by bare B_5N_{10} (Ahluwalia, 2023; Herreros & Harbison, 2002):

$$V(r) = V(0) + \left[\left(\frac{\partial V}{\partial x_i}\right)\Big|_{0} .x_i\right] + \frac{1}{2}\left[\left(\frac{\partial^2 V}{\partial x_i x_j}\right)\Big|_{0} .x_i x_j\right] + \dots \tag{9}$$

$$\begin{aligned} U &= -\tfrac{1}{2}\int\limits_D d^3 r \rho_r \left[\left(\tfrac{\partial^2 V}{\partial x_i^2}\right)\Big|_0 \cdot x_i^2\right] = \\ &= \int\limits_D d^3 r \rho_r \left[\left(\tfrac{\partial^2 V}{\partial x_i^2}\right)\Big|_0 \cdot x_i^2\right] = -\tfrac{1}{2}\left(\tfrac{\partial^2 V}{\partial x_i^2}\right)\Big|_0 \int\limits_D d^3 r \left[\rho(r)\cdot x_i^2\right] \end{aligned} \tag{10}$$

$$\chi = {e^2 Q q_{zz}}/{h}, \tag{11}$$

$$\eta = {q_{xx} - q_{yy}}/{q_{zz}}. \tag{12}$$

Table 1: The amounts of electric potential (Ep /a.u.) and Bader charge (Q /coulomb) through NQR calculation for Cr@B_5N_{10}, Mn@B_5N_{10}, Fe@B_5N_{10}, Zn@B_5N_{10}, W@B_5N_{10}, and Cd@B_5N_{10} complexes.

Cr@B_5N_{10}			Mn@B_5N_{10}			Fe@B_5N_{10}		
Atom	Q	Ep	Atom	Q	Ep	Atom	Q	Ep
B1	0.2828	–11.2393	B1	0.1887	–11.2193	B1	0.2717	–11.2441
N2	–0.2049	–18.105	N2	–0.0523	–18.282	N2	–0.1845	–18.0895
N3	–0.2541	–18.1164	N3	–0.1655	–18.3053	N3	–0.2511	–18.1138
B4	0.3299	–11.2321	B4	0.2017	–11.216	B4	0.3140	–11.2473
B5	0.3201	–11.2409	B5	0.2274	–11.2108	B5	0.3133	–11.2418
B6	0.3188	–11.2218	B6	0.1993	–11.214	B6	0.2786	–11.2448
N7	–0.1983	–18.1174	N7	–0.0548	–18.2828	N7	–0.1739	–18.1000
N8	–0.2688	–18.1262	N8	–0.1643	–18.2941	N8	–0.2434	–18.1089
N9	–0.3384	–18.1411	N9	–0.0516	–18.2949	N9	–0.3647	–18.1450
N10	–0.3121	–18.1349	N10	–0.0570	–18.291	N10	–0.3191	–18.1405
N11	–0.2881	–18.1448	N11	–0.0701	–18.2889	N11	–0.2773	–18.1317
N12	–0.3654	–18.1287	N12	–0.0798	–18.2973	N12	–0.3987	–18.1326
B13	0.1103	–11.2455	B13	0.3039	–11.2192	B13	–0.0212	–11.2706
N14	–0.1623	–18.0959	N14	–0.1153	–18.2945	N14	–0.1363	–18.0795
N15	–0.1702	–18.1124	N15	–0.1382	–18.293	N15	–0.1591	–18.0975
Cr16	1.2008	–101.752	Mn16	–0.1721	–16.5602	Fe16	1.3518	–113.9002
Zn@B_5N_{10}			W@B_5N_{10}			Cd@B_5N_{10}		
Atom	Q	Ep	Atom	Q	Ep	Atom	Q	Ep
B1	0.2799	–11.2520	B1	0.2011	–11.2204	B1	0.2777	–11.2438
N2	–0.2288	–18.1241	N2	–0.0759	–18.2918	N2	–0.2465	–18.1376
N3	–0.2132	–18.1010	N3	–0.2086	–18.3087	N3	–0.2229	–18.0972
B4	0.3237	–11.2448	B4	0.2295	–11.2118	B4	0.3237	–11.2384
B5	0.3168	–11.2466	B5	0.2541	–11.2091	B5	0.3014	–11.2511
B6	0.2980	–11.2448	B6	0.2326	–11.2120	B6	0.2946	–11.2431
N7	–0.1943	–18.1118	N7	–0.0460	–18.2929	N7	–0.2207	–18.1338
N8	–0.2260	–18.0996	N8	–0.2068	–18.3070	N8	–0.2303	–18.1073
N9	–0.3150	–18.1335	N9	–0.1994	–18.3165	N9	–0.3292	–18.1283
N10	–0.2951	–18.1390	N10	–0.1921	–18.3082	N10	–0.3202	–18.1389
N11	–0.2585	–18.1334	N11	–0.2121	–18.3019	N11	–0.2763	–18.1419
N12	–0.3695	–18.1353	N12	–0.2191	–18.3161	N12	–0.4067	–18.1296
B13	0.0617	–11.2438	B13	0.4340	–11.2307	B13	0.0513	–11.2051
N14	–0.1729	–18.1144	N14	–0.0319	–18.2847	N14	–0.1703	–18.1083
N15	-0.1664	–18.1025	N15	–0.0755	–18.2875	N15	–0.1538	–18.1018
Zn16	1.1597	–139.8870	W16	0.1162	–10.3367	Cd16	1.3286	–268.156

Since the electric field gradient (EFG) at the settlement of the nucleus in metal atoms including Cr, Mn, Fe, Zn, W, Cd is defined by the valence electrons bent in the pure location

with familiar nuclei of bare B_5N_{10} through trapping of Cr, Mn, Fe, Zn, W, Cd, the frequency of NQR at which intermediates occur is only for X@B_5N_{10} complexes (X = Cr, Mn, Fe, Zn, W, Cd) (Table 1). In the present research, the electric potential via Bader charge was estimated for Cr@B_5N_{10}, Mn@B_5N_{10}, Fe@B_5N_{10}, Zn@B_5N_{10}, W@B_5N_{10}, and Cd@B_5N_{10} complexes (Table 1).

Furthermore, in Figure 5 (a–f), the graph of electric potential fluctuation via Bader charge for toxic TMs including Cr, Mn, Fe, Zn, W, Cd grabbed by the B_5N_{10} have been assessed.

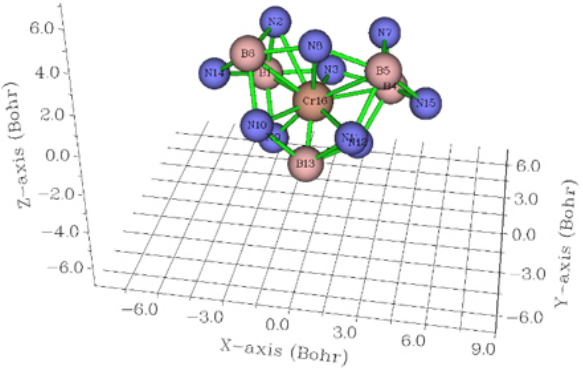

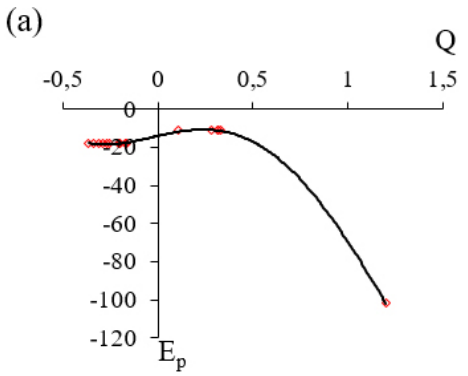

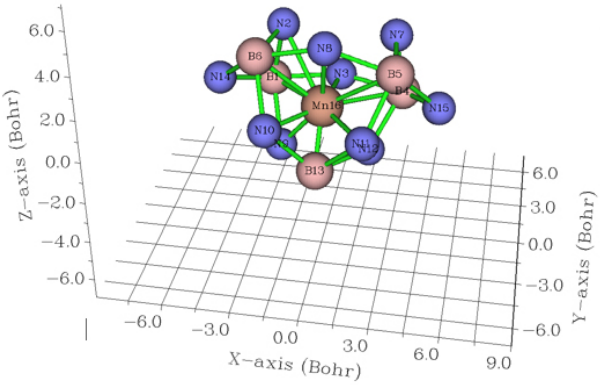

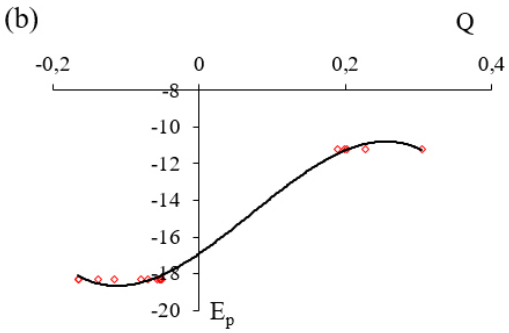

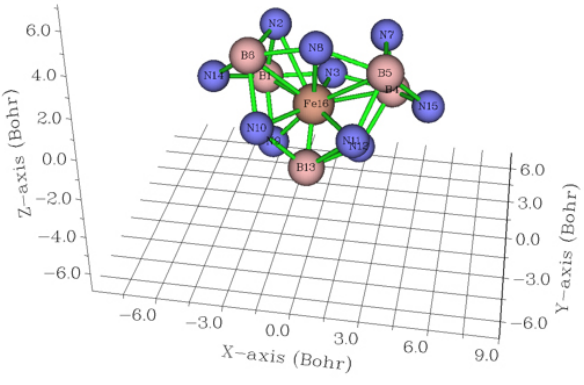

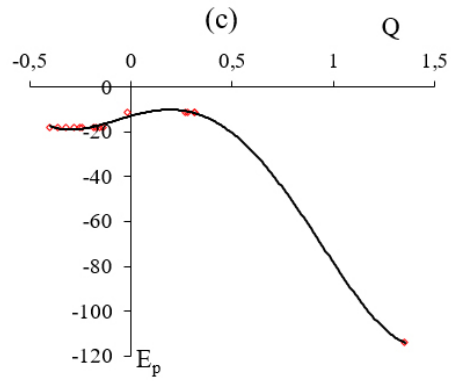

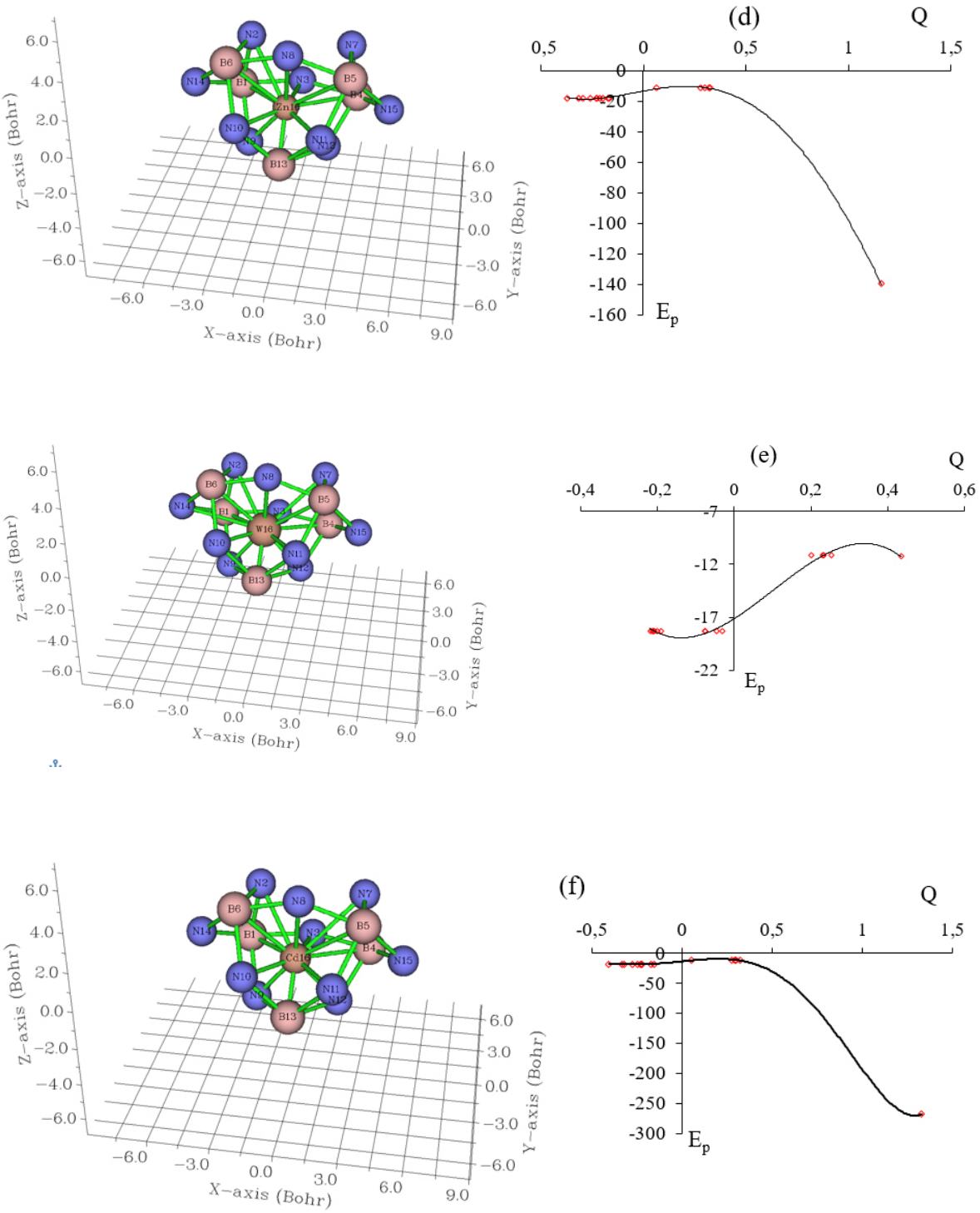

Figure 5: The amounts of electric potential (Ep/a.u.) versus Bader charge (Q/coulomb) through NQR calculation for complexes of a- Cr@B_5N_{10}, b- Mn@B_5N_{10}, c- Fe@B_5N_{10}, d- Zn@B_5N_{10}, e- W@B_5N_{10}, and f- Cd@B_5N_{10}

.

In Figure 5 (a–f), the trapping fluctuation of Cr, Mn, Fe, Zn, W, Cd by bare B_5N_{10} for sensing the toxic metal atoms in the contaminated soil can be observed. The graph of bare B_5N_{10} is bent by these toxic atoms. The sharpest curves for electric potential were nominated for metal atoms trapped by the bare B_5N_{10} that prove the electron attaining of these elements aided by boron and nitrogen atoms of bare B_5N_{10} based on the relation coefficient of R^2 as:

$Cd@B_5N_{10} > Zn@B_5N_{10} \approx Cr@B_5N_{10} > Fe@B_5N_{10} > Mn@B_5N_{10} > W@B_5N_{10}$ (Figure 5a–f).

3.4 Application of Nuclear Magnetic Resonance (NMR)

As a matter of fact, magnetic field gradients fix it feasible to tag spatial coordinates within a model. The frequencies resonance of most atoms is well segregated from each other which causes NMR to be an element-specific method. Interactions of spins with their local environment direct spectral alterations that evoke the local geometry and physico-chemical states. Therefore, NMR spectrum of bare B_5N_{10} for trapping metal atoms containing Cr, Mn, Fe, Zn, W, Cd might illustrate the possibility of bare B_5N_{10} for sensing and grabbing of these toxic elements from contaminated soil toward measuring the isotropic chemical-shielding (CSI) and anisotropic chemical-shielding (CSA) (Sarasia et al., 2011; Mollaamin & Monajjemi, 2023; Bakhshi et al., 2011; Tahan et al., 2009):

$$\sigma_{iso} = (\sigma_{11} + \sigma_{22} + \sigma_{33})/3 \tag{13}$$

$$\sigma_{aniso} = \sigma_{33} - (\sigma_{22} + \sigma_{11})/2 \tag{14}$$

The NMR quantities of isotropic (σiso) and anisotropic shielding tensor (σ aniso) of Ba, As, Se, Co, Cu, Mo trapped on the in the bare B_5N_{10} towards formation of Cr@B_5N_{10}, Mn@B_5N_{10}, Fe@B_5N_{10}, Zn@B_5N_{10}, W@B_5N_{10}, and Cd@B_5N_{10} complexes was computed by Gaussian 16 revision C.01 program package (Table 2).

Table 2 has reported NMR amounts for TMs including Cr, Mn, Fe, Zn, W, Cd encapsulated in the bare B_5N_{10}. Grabbing Cr, Mn, Fe, Zn, W, Cd shows the spin polarization on the (Cr, Mn, Fe, Zn, W, Cd)–encapsulated bare B_5N_{10}. The increase in the chemical shift anisotropy spans for atom trapping by the bare B_5N_{10} are near $N(2), N(3), N(7), N(8), N(9), N(10), N(11), N(12)$, $N(14)$ $N(15)$ (Table 2). The observed weak signal intensity near the parallel edge of the nanocage might be owing to boron binding induced non-spherical distribution of these complexes. It is obvious that grabbing Cr, Mn, Fe, Zn, W, Cd by bare B_5N_{10} might promote the strength of the nanocage that concludes an increase in the magnetic of clusters (Table 2).

Figure 6(a–f) indicated the same desire of shielding factor for boron and nitrogen; however, a remarkable deviation is observed from trapping atoms of Cr (6) (Figure 6a), Mn (16), (Figure 6b), Fe (16) (Figure 6c), Zn (16) (Figure 6d), W (16) (Figure 6e), Cd (16) (Figure 6f) through interaction with boron and nitrogen of bare B_5N_{10}.

In Figure 6 (a–f), toxic elements of Cr, Mn, Fe, Zn, W, Cd in the complexes of Cr@B_5N_{10} (Figure 6a), Mn@B_5N_{10} (Figure 6b), Fe@B_5N_{10} (Figure 6c), Zn@B_5N_{10} (Figure 6d), W@B_5N_{10} (Figure 6e), and Cd@B_5N_{10} (Figure 6f) describe the oscillation in the chemical shielding during atom capture.

Figure 6 (a–f) defines the chemical shielding between boron/nitrogen in bare B_5N_{10} and metal atoms. Thus, it may be brought up that the turnover of electron admitting for the captured toxic atoms in the bare B_5N_{10}- is $Cd > Zn > Fe > Mn > Cr \approx W$ that proves the strength of covalent bond across boron/nitrogen and these elements toward atom catching.

Table 2: Data of NMR shielding tensors for selected atoms of Cr@B_5N_{10}, Mn@B_5N_{10}, Fe@B_5N_{10}, Zn@B_5N_{10}, W@B_5N_{10}, and Cd@B_5N_{10} complexes using CAM–B3LYP–D3/LANL2DZ calculations.

Cr @ B_5N_{10}			Mn @ B_5N_{10}			Fe @ B_5N_{10}		
Atom	σiso	σaniso	Atom	σiso	σaniso	Atom	σiso	σaniso
B1	117.0076	83.0844	B1	93.1958	74.3373	B1	136.1640	112.1263
N2	99.8785	287.9554	N2	107.1708	412.4542	N2	252.7308	554.3353
N3	38.3300	429.4735	N3	288.8404	780.6410	N3	163.8389	480.5763
B4	109.5591	90.4106	B4	98.4627	54.7623	B4	137.8643	110.5202
B5	104.4110	97.3531	B5	80.4756	75.4378	B5	125.1732	101.4723
B6	84.1512	70.3800	B6	80.8233	69.2619	B6	137.0509	99.3871
N7	65.8298	250.6901	N7	111.0482	258.3691	N7	76.0677	523.9335
N8	173.4262	711.3619	N8	359.3933	935.9902	N8	5.1401	118.9943
N9	228.2622	477.9766	N9	390.0925	580.1841	N9	11.8325	408.4318
N10	297.3492	970.5455	N10	353.0870	404.1981	N10	15.6186	277.7235
N11	112.1550	469.8254	N11	122.8970	484.1625	N11	8.1861	651.2432
N12	146.1509	520.7535	N12	126.0121	403.8011	N12	40.8260	366.0072
B13	23.4107	161.6682	B13	51.7642	125.5008	B13	92.9565	56.1805
N14	61.4369	542.2817	N14	390.1933	1289.4891	N14	137.8765	620.3838
N15	144.2153	582.4029	N15	281.0691	1330.1789	N15	66.2572	524.5995
Cr16	8.8171	531.8666	Mn16	4675.2397	3740.2405	Fe16	982.3792	1080.9150
Zn @ B_5N_{10}			W @ B_5N_{10}			Cd @ B_5N_{10}		
Atom	σiso	σaniso	Atom	σiso	σaniso	Atom	σiso	σaniso
B1	130.5100	91.8778	B1	91.6888	68.8491	B1	127.2884	98.7797
N2	21.6821	546.0132	N2	23.4058	244.5637	N2	14.3171	555.9098
N3	56.0171	57.5374	N3	223.6585	505.2747	N3	13.4107	122.4605
B4	120.3790	53.0462	B4	92.2361	72.9567	B4	103.1204	115.3330
B5	115.0078	68.5589	B5	81.6149	72.3481	B5	118.2561	61.9536
B6	133.6303	81.2506	B6	79.3710	80.4153	B6	123.6742	80.8870
N7	1.3263	478.3851	N7	67.1424	230.3649	N7	131.6130	549.6007
N8	51.1373	184.3061	N8	331.0739	856.4636	N8	19.8739	130.0665
N9	134.4198	330.9866	N9	454.0576	614.2209	N9	97.3508	203.8768
N10	55.0733	270.0957	N10	432.1887	652.7413	N10	41.2612	585.3871
N11	35.5475	334.9535	N11	276.3243	480.2979	N11	26.8124	253.2975
N12	166.1786	238.3185	N12	133.3741	462.9130	N12	25.7318	620.6356
B13	126.7224	17.4660	B13	17.5072	225.2369	B13	139.3014	55.8459
N14	32.3937	478.1249	N14	413.1482	983.4193	N14	47.7721	423.7621
N15	104.9527	596.0890	N15	381.9037	1002.6071	N15	92.9321	392.1182
Zn16	2920.2381	3680.6586	W16	37.9252	77.2940	Cd16	3945.3535	242.5438

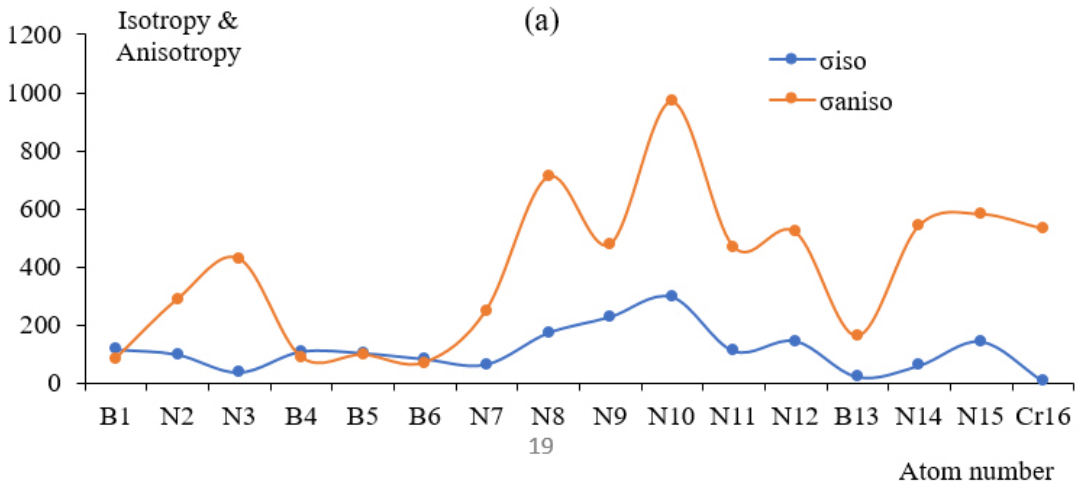

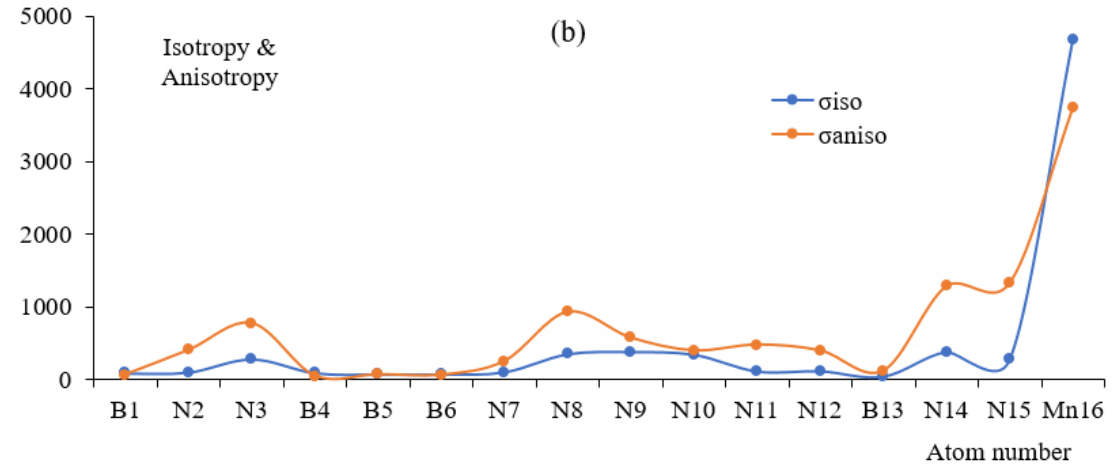
(b)
Isotropy &
Anisotropy
σiso
σaniso
5000
4000
3000
2000
1000
0
B1 N2 N3 B4 B5 B6 N7 N8 N9 N10 N11 N12 B13 N14 N15 Mn16
Atom number

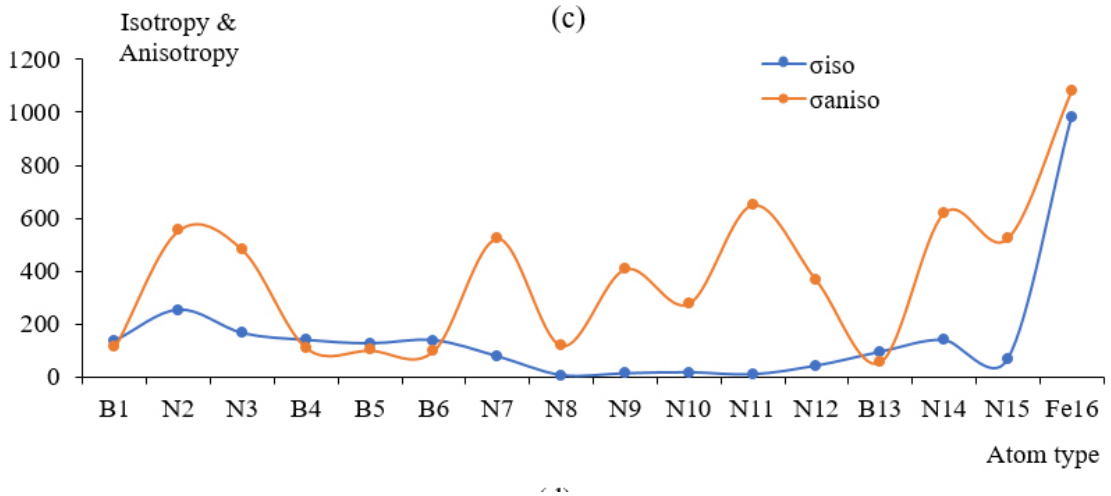
(c)
Isotropy &
Anisotropy
σiso
σaniso
1200
1000
800
600
400
200
0
B1 N2 N3 B4 B5 B6 N7 N8 N9 N10 N11 N12 B13 N14 N15 Fe16
Atom type

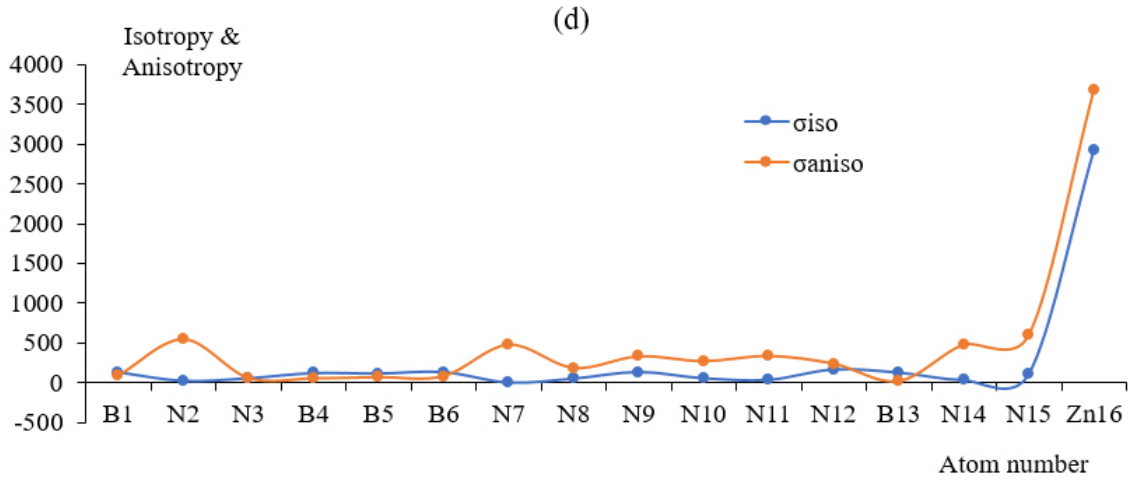
(d)
Isotropy &
Anisotropy
σiso
σaniso
4000
3500
3000
2500
2000
1500
1000
500
0
-500
B1 N2 N3 B4 B5 B6 N7 N8 N9 N10 N11 N12 B13 N14 N15 Zn16
Atom number

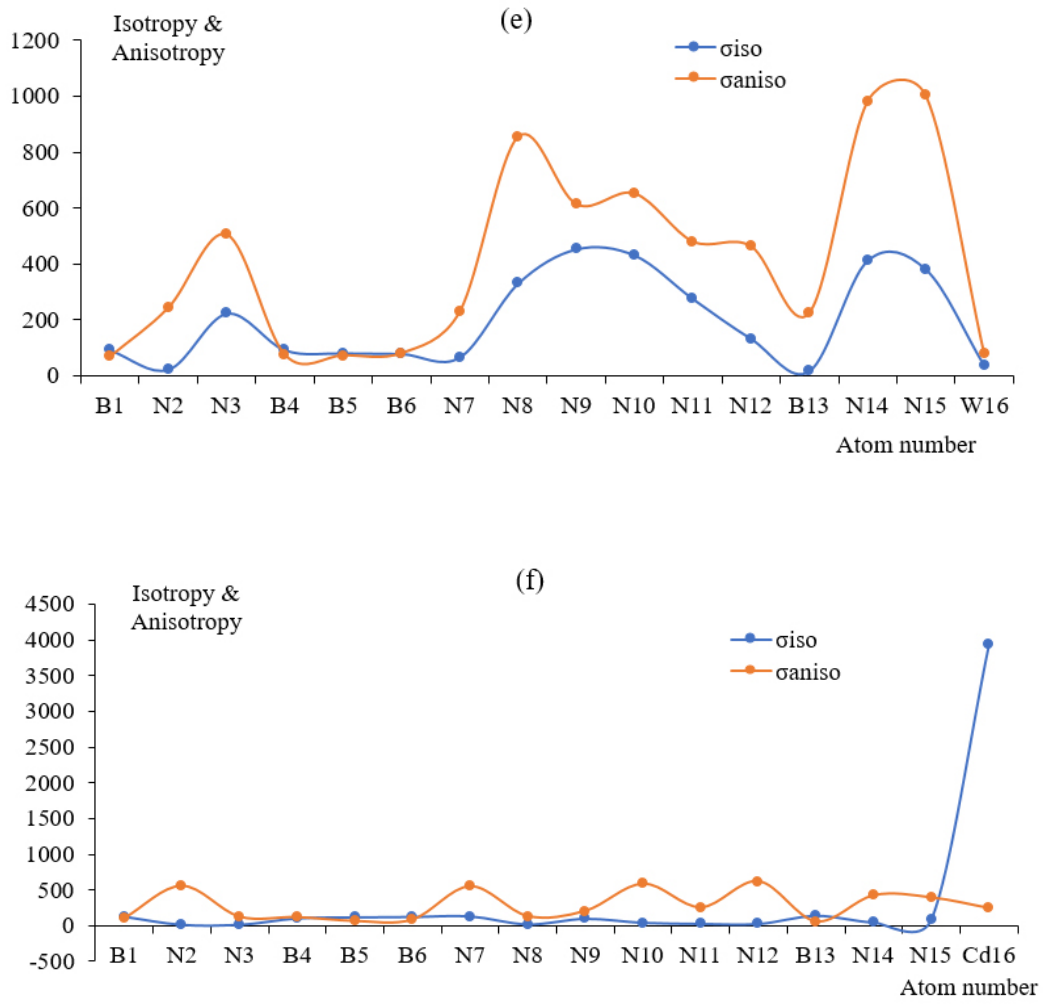

Figure 6: The NMR spectrum for complexes of $a-$ Cr@B_5N_{10}, $b-$ Mn@B_5N_{10}, $c-$ Fe@B_5N_{10}, $d-$ Zn@B_5N_{10}, $e-$ W@B_5N_{10}, and $f-$ Cd@B_5N_{10} using CAM–B3LYP–D3/LANL2DZ.

3.5 Analysis of Infrared (IR) Spectra

Encapsulating TMs including Cr, Mn, Fe, Zn, W, Cd in the bare B_5N_{10} has been evaluated by IR spectroscopy during atom sensing in soil. The complexes of Cr@B_5N_{10} (Figure 7a), Mn@B_5N_{10} (Figure 7b), Fe@B_5N_{10} (Figure 7c), Zn@B_5N_{10} (Figure 7d), W@B_5N_{10} (Figure 7e), and Cd@B_5N_{10} (Figure 7f) have been analyzed through the IR spectroscopy.

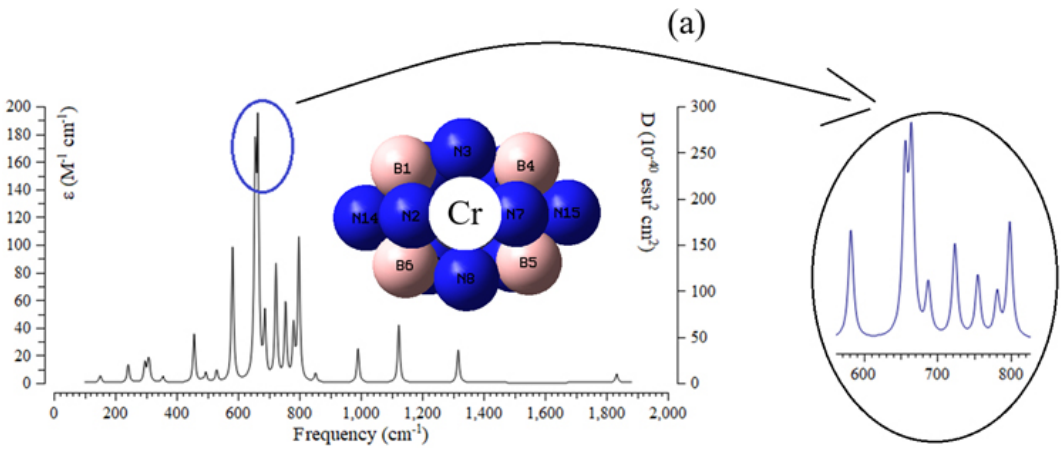

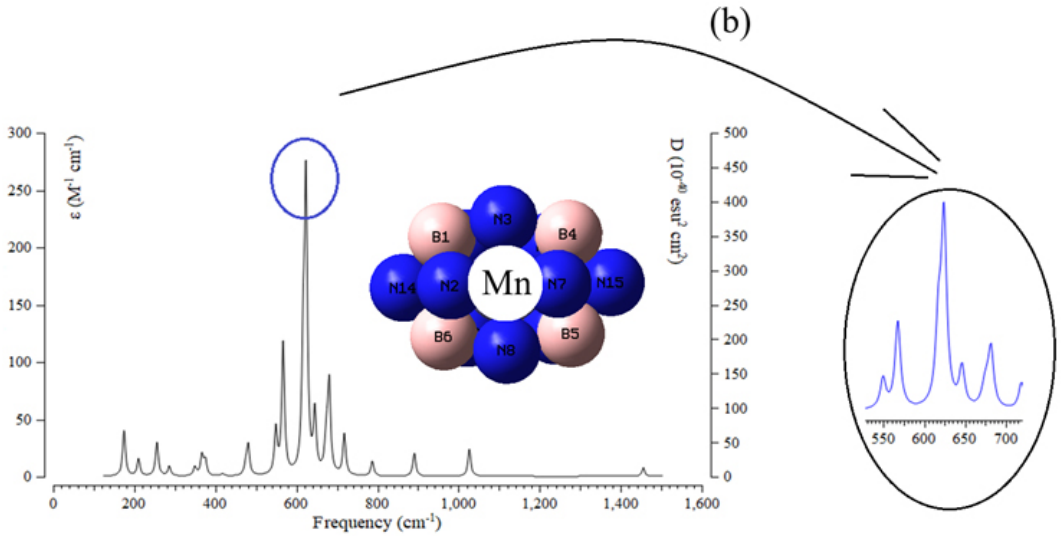
(b)
ε (M⁻¹ cm⁻¹)
D (10⁻⁴⁰ esu² cm²)
Frequency (cm⁻¹)
Mn
B1
N3
B4
N14
N2
N7
N15
B6
N8
B5

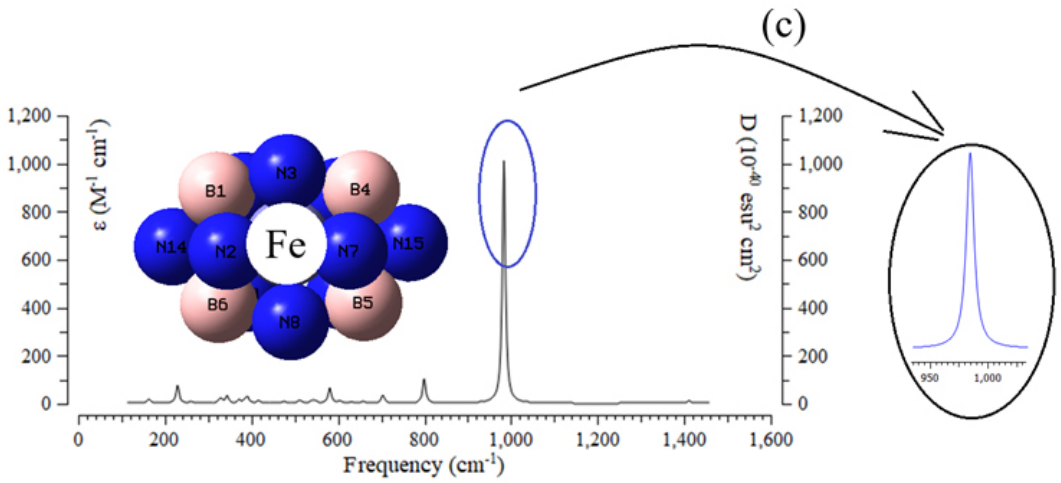
(c)
ε (M⁻¹ cm⁻¹)
D (10⁻⁴⁰ esu² cm²)
Frequency (cm⁻¹)
Fe
B1
N3
B4
N14
N2
N7
N15
B6
N8
B5

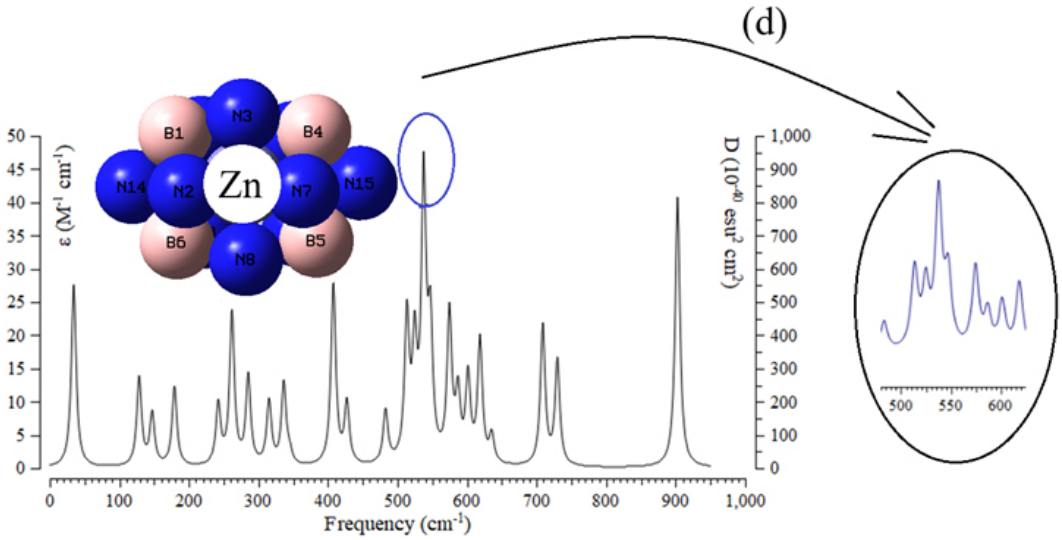
(d)
ε (M⁻¹ cm⁻¹)
D (10⁻⁴⁰ esu² cm²)
Frequency (cm⁻¹)
Zn
B1
N3
B4
N14
N2
N7
N15
B6
N8
B5

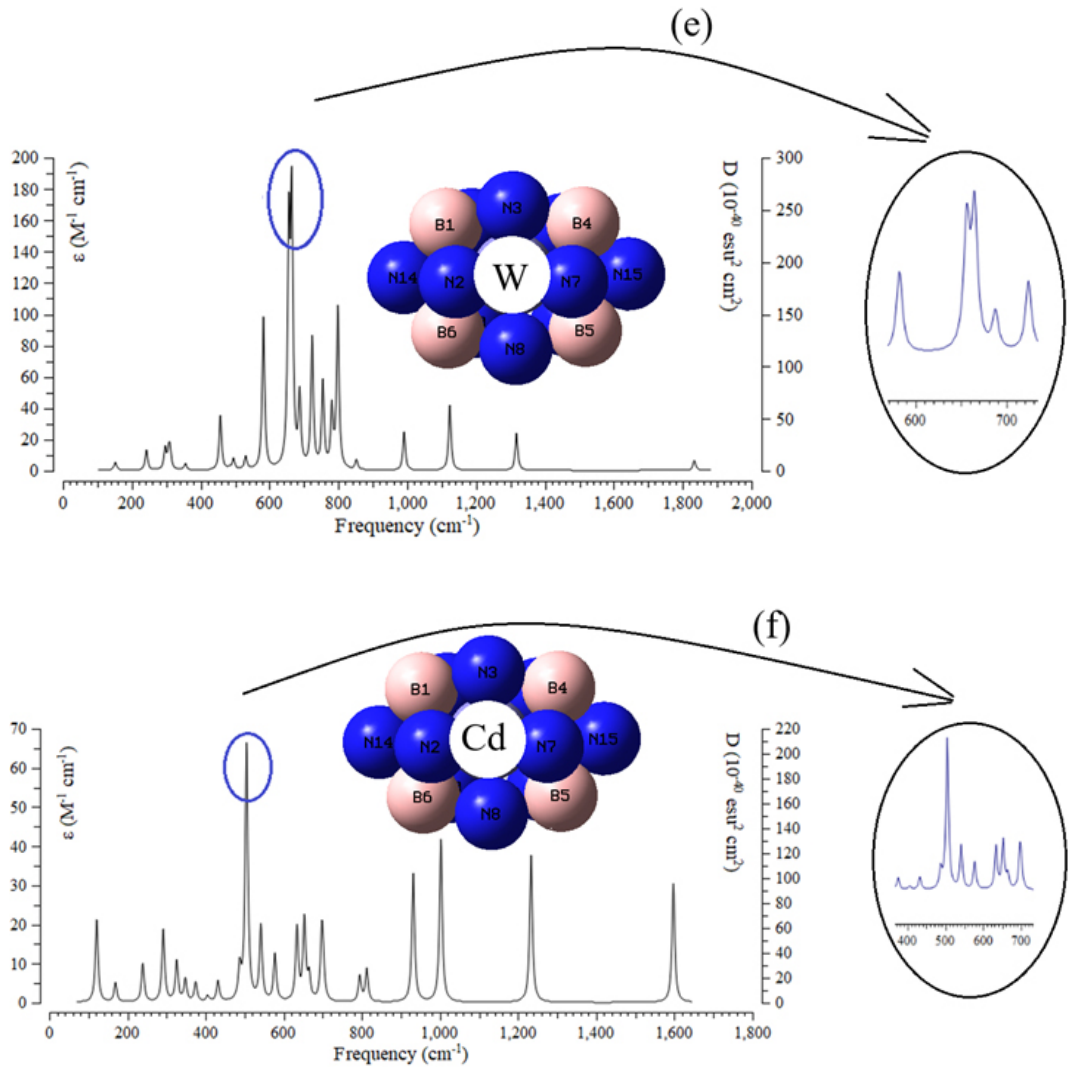

Figure 7: IR spectra for complexes of $a-$ Cr@B_5N_{10}, $b-$ Mn@B_5N_{10}, $c-$ Fe@B_5N_{10}, $d-$ Zn@B_5N_{10}, $e-$ W@B_5N_{10}, and $f-$ Cd@B_5N_{10} complexes.

The graph of Figure 7(a) has been shown in the frequency about $200 - -1800cm^{-1}$ for Cr@B_5N_{10} with several sharp peaks around 655.26, 691.58, and $714.46cm^{-1}$. Then, Figure 7(b) was shown in the frequency limitation across 200–1100 cm^{-1} for Mn@B_5N_{10} with several sharp peaks around 567.21, 616.88, 623.54, and 680.89 cm^{-1}. Figure 7(c) has indicated the frequency around 1800–1100 cm^{-1} for Fe@B_5N_{10} with one sharp peak around 983.42 cm^{-1}. Figure 7(d) has shown the fluctuation frequency between 50–950 cm^{-1} for Zn@B_5N_{10} with two sharp peaks around 537.66 and 902.68 cm^{-1}. Figure 7(e) has indicated the fluctuation of frequency between 200–1400 cm^{-1} for W@B_5N_{10} with several sharp peaks around 582.28, 656.11, 664.63, 723.76, and 798.39 cm^{-1}. Figure 7(f) has shown the frequency range between 100–1600 cm^{-1} for Cd@B_5N_{10} with several sharp peaks around 504.75, 1002.32, and 1233.14 cm^{-1}. Table 3 has described that the bare B_5N_{10} owing to capture TMs including Cr, Mn, Fe, Zn, W, Cd might be more efficient detector for sensing and catching these elements from soil.

Table 3: The thermochemical characters of bare B_5N_{10} and encapsulated derivatives of Cr@B_5N_{10}, Mn@ B_5N_{10}, Fe@ B_5N_{10}, Zn@B_5N_{10}, W@B_5N_{10}, and Cd@B_5N_{10} complexes.

Compound	$E_b^0 \times 10^{-3}$ (kcal/mol)	$\Delta E^0 \times 10^{-3}$ (kcal/mol)	$\Delta H^0 \times 10^{-3}$ (kcal/mol)	$\Delta G^0 \times 10^{-3}$ (kcal/mol)	Dipole moment (Debye)
bare B_5N_{10}	–420.550	0	–420.549	–420.579	0.2020
Cr@B_5N_{10}	–1063.754	–643.204	–1063.754	–1063.782	0.6941
Mn@B_5N_{10}	–485.602	–65.052	–485.602	–485.629	0.4888
Fe@B_5N_{10}	–1199.586	–779.036	–1199.585	–1199.614	1.4484
Zn@B_5N_{10}	–1518.749	–1098.199	–1518.748	–1518.780	0.9416
W@B_5N_{10}	–462.747	–42.197	–462.746	–462.774	0.5946
Cd@B_5N_{10}	–3811.957	–3391.407	–3811.957	–3811.985	0.7560

Table 3 could introduce the ability of metal elements of Cr, Mn, Fe, Zn, W, Cd trapped in the bare B_5N_{10} through thermodynamic properties of thermal entropy ($\triangle H^o$), Gibbs free energy ($\triangle G^o$), stability energy ($\triangle E^0$), and binding energy (E_b^o), which are related to the covalent bond between these elements and bare B_5N_{10} as a potent detector for soil purification.

The trapping process of metal elements including Cr, Mn, Fe, Zn, W, Cd in the bare B_5N_{10} is affirmed by the $\triangle G_{ads}^o$ quantities:

$$\Delta G_{adc}^o = \Delta G_{X@B_5N_{10}}^o - \left(\Delta G_{X-grabbed}^o + \Delta G_{B_5N_{10}}^o\right); \quad X = Cr, Mn, Fe, Zn, W, Cd. \tag{15}$$

Furthermore, Table 3 has shown that the dependence on the size of the atoms of during interaction between the adsorbates of the metal elements as the electron acceptors and the adsorbent of B_5N_{10} as electron donor in the complexes of Cr@B_5N_{10}, Mn@B_5N_{10}, Fe@B_5N_{10}, Zn@B_5N_{10}, W@B_5N_{10}, and Cd@B_5N_{10}.

4 Conclusion

Encapsulated transition metal has exhibited excellent performance for elimination of contamination due to their unique physicochemical properties. Taking advantage of the synergy between transition metal nanoparticles and encapsulation materials, stability and selectivity of them can be adjusted and improved. B_5N_{10} can be used to capture metal elements from soil because of electrostatic interactions between metal elements and bare B_5N_{10}. The thermochemistry and electromagnetic parameters of Cr, Mn, Fe, Zn, W, Cd absorbed bare B_5N_{10} has been illustrated by DFT method. The consequences have defined that Cr, Mn, Fe, Zn, W, Cd trapped in bare B_5N_{10} are rather fixed with the most stable adsorption site being in the center of bare B_5N_{10} system. Catching Cr, Mn, Fe, Zn, W, Cd in the B_5N_{10} happens due to chemisorption phenomenon. The n-grabbing behavior can be found in B_5N_{10} after the adsorption of Cr, Mn, Fe, Zn, W, Cd. The work function of bare B_5N_{10} has remarkably exhibited the TMs trapping with maximum amount for the $Cd > Zn > Fe > Cr > Mn \approx W$ –adsorbed bare B_5N_{10} system. Moreover, it is proposed that TMs capture can be employed to design and progress the optoelectronic specification of bare B_5N_{10} for inventing photoelectric instruments. This research article presents the structure and composition types of encapsulated transition metal boron nitride and then it concludes by highlighting the major challenges and opportunities associated with encapsulated transition-metal nanoparticle providing valuable insights for future research and development.

Acknowledgements

In successfully completing this paper and its research, the authors are grateful to Kastamonu University.

References

Ahluwalia, V.K. (2023). Nuclear Quadrupole Resonance (NQR) Spectroscopy. In: *Instrumental Methods of Chemical Analysis*. Springer, Cham.451-456. https://doi.org/10.1007/978-3-031-38355-7_30.

Al-Makishah, N.H., Taleb, M.A. & Barakat, M.A. (2020). Arsenic bioaccumulation in arsenic-contaminated soil: a review. *Chem. Pap.,* 74, 2743–2757. https://doi.org/10.1007/s11696-020-01122-4

Bader, R.F.W. (2001). The zero-flux surface and the topological and quantum definitions of an atom in a molecule. Theor. Chem. Accounts, 105, 276-283. https://doi.org/10.1007/s002140000233

Bakhshi, K., Mollaamin, F. & Monajjemi, M. (2011). Exchange and correlation effect of hydrogen chemisorption on nano V (100) surface: A DFT study by generalized gradient approximation (GGA). *Journal of Computational and Theoretical Nanoscience*, *8*(4), 763-768. https://doi.org/10.1166/jctn.2011.1750

Becke, A.D. (1993). Density-functional thermochemistry. III. The role of exact exchange. *The Journal of Chemical Physics, 98*(7), 5648-5652. https://doi.org/10.1063/1.464913

Becke, A.D., Edgecombe, K.E. (1990). A simple measure of electron localization in atomic and molecular systems. *J. Chem. Phys. 92*, 5397-5403. https://doi.org/10.1063/1.458517

Chao, Y.H., Zhang, J., Li, H.P., Wu, P.W., Li, X.W., Chang, H.H., He, J., Wu, H.F., Li, H.M., Zhu, W.S. (2020). Synthesis of boron nitride nanosheets with N-defects for efficient tetracycline antibiotics adsorptive removal. *Chem. Eng. J.*, *387*, 124138. https://doi.org/10.1016/j.cej.2020.124138

Cramer, C.J. (2013). *Essentials of Computational Chemistry: Theories and Models*. John Wiley & Sons.

Da Silva, E.B., Gao, P., Xu, M., Guan, D., Tang, X., & Ma, L.Q. (2010). Background concentrations of trace metals As, Ba, Cd, Co, Cu, Ni, Pb, Se, and Zn in 214 Florida urban soils: Different cities and land uses. *Environmental Pollution*, *264*, 114737. https://doi.org/10.1016/j.envpol.2020.114737

Davies, A., Albar, J.D., Summerfield, A., Thomas, J.C., Cheng, T.S., Korolkov, V.V., Stapleton, E., Wrigley, J., Goodey, N.L., & Mellor, C.J. (2018). Lattice-Matched Epitaxial Graphene Grown on Boron Nitride. *Nano Lett.*, *18*, 498-504. https://doi.org/10.1021/acs.nanolett.7b04453

De Miguel, E., De Grado, M.J., Llamas, J.F., Martín-Dorado, A., Mazadiego, L.F.(1998). The overlooked contribution of compost application to the trace elements in playgrounds in Madrid (Spain). *Sci. Total Environ*, *215*, 113-122. https://doi.org/10.1016/S0048-9697(98)00112-0.

Dennington, R.D.I.I., Keith, T.A. & Millam, J.M. (2016). GaussView, version 6.0.16. Semichem Inc Shawnee Mission KS.

Frisch, M.J., Trucks, G.W., Schlegel, H.B., Scuseria, G.E. & Robb, M.A. (2016). Gaussian 16. Revision C.01.

Grimme, S., Antony, J., Ehrlich, S. & Krieg, H. (2010). A consistent and accurate ab initio parametrization of density functional dispersion correction (DFT-D) for the 94 elements H-Pu. *The Journal of Chemical Physics*, *132*(15). https://doi.org/10.1063/1.3382344

Grimme, S., Ehrlich, S., & Goerigk, L., (2011). Effect of the damping function in dispersion corrected density functional theory. *J Comput Chem.*, *32*(7), 1456-65. https://doi.org/10.1002/jcc.21759

Guo, Y., Wang, R.X., Wang, P.F., Rao, L.,& Wang, C. (2019). Developing a novel layered boron nitride-carbon nitride composite with high efficiency and selectivity to remove protonated dyes from water. *ACS Sustain. Chem.*, *7* (6), 5727-5741. https://doi.org/10.1021/ACSSUSCHEMENG.8B05150

Henkelman, G., Arnaldsson, A. & Jónsson, H. (2006). A fast and robust algorithm for Bader decomposition of charge density. *Computational Materials Science*, *36*(3), 354-360. https://doi.org/10.1016/j.commatsci.2005.04.010

Herreros, B., Harbison, G.S. (2002). Nuclear Quadrupole Resonance, *Characterization of Materials*, 1st ed., *2*, 775-792, by, University of Nebraska, Lincoln, Nebraska; Published online. https://doi.org/10.1002/0471266965.com066

Hohenberg, P., Kohn, W. (1964). Inhomogeneous electron gas. *Physical Review*, *136*(3B), B864. https://doi.org/10.1103/PhysRev.136.B864

Ji, K., Kim, J.K., Lee, M.J., Park, S.Y., Kwon, H.J., Cheong, H.K., Jang, J.Y., Kim, D.S., Yu, S., & Kim, Y.W. (2013). Assessment of exposure to heavy metals and health risks among residents near abandoned metal mines in Goseong, Korea. *Environ. Pollut.* , *178*, 322-328. https://doi.org/10.1016/j.envpol.2013.03.031

Jiang, M., Wang, K., Wang, Y., Zhao, Q., & Wang, W. (2022). Technologies for the cobalt-contaminated soil remediation: A review. *Science of The Total Environment*, *813*, 151908. https://doi.org/10.1016/j.scitotenv.2021.151908

Kachenko, A.G., Singh, B. (2006). Heavy metals contamination in vegetables grown in urban and metal smelter contaminated sites in Australia. *Water Air Soil Pollut.*, *169*, 101-123. https://doi.org/10.1007/s11270-006-2027-1

Kim, S., Cho, Y.M., Choi, S.H., Kim, H.J., & Choi, J. (2011). The effect of exposure factors on the concentration of heavy metals in residents near abandoned metal mines. *J. Prev. Med. Public Health*, *44*, 41–47. https://doi.org/10.3961/jpmph.2011.44.1.41

Kim, K., Jordan, K.D. (1994). Comparison of density functional and MP2 calculations on the water monomer and dimer. *The Journal of Physical Chemistry*, *98*(40), 10089-10094 https://doi.org/10094.10.1021/j100091a024

Kohn, W., Sham, L.J. (1965). Self-consistent equations including exchange and correlation effects. *Physical Review*, *140*(4A), A1133. https://doi.org/10.1103/PhysRev.140.A1133

Lee, C., Yang, W. & Parr, R.G. (1988). Development of the Colle-Salvetti correlation-energy formula into a functional of the electron density. *Physical review B*, *37*(2), 785. https://doi.org/10.1103/PhysRevB.37.785

Li, C., Zhou, K., Qin, W., Tian, C., Qi, M., Yan, X. & Wenbing Han, W. (2019). A Review on Heavy Metals Contamination in Soil: Effects, Sources, and Remediation Techniques. *Soil and Sediment Contamination: An International Journal*, *28*(4), 380-394. https://doi.org/10.1080/15320383.2019.1592108

Li, Y., Gou, X., Wang, G., Zhang, Q., Su, Q., Xiao, G. (2008). Heavy metal contamination and source in arid agricultural soils in central Gansu province, China. *J. Environ. Sci.*, *20*, 607-612. https://doi.org/10.1016/S1001-0742(08)62101-4

Liu, H., Probst, A., & Liao, B. (2005). Metal contamination of soils and crops affected by the Chenzhou lead/zinc mine spill (Hunan, China). *Sci. Total Environ.*, *339*, 153-166. https://doi.org/10.1016/j.scitotenv.2004.07.030

Liu, W.X., Shen, L.F., Liu, J.W., Wang, Y.W., & Li, S.R. (2007). Uptake of toxic heavy metals by rice (*Oryza sativa* L.) cultivated in the agricultural soils near Zhengzhou City. People's Republic of China. *Bull. Environ. Contam. Toxicol*, *79*, 209-213. https://doi.org/10.1007/s00128-007-9164-0

Lu, T., Chen, F. (2012). Multiwfn: A multifunctional wavefunction analyzer. *J. Comput. Chem. 33*, 580-592. https://doi.org/10.1002/jcc.22885

Lu, T. (2024). A comprehensive electron wavefunction analysis toolbox for chemists, Multiwfn. *J. Chem. Phys., 161*, 082503. https://doi.org/10.1063/5.0216272

Madrid, L., Díaz-Barrientos, F., & Madrid, F. (2002). Distribution of heavy metal contents of urban soils in parks of Seville. *Chemosphere*, *49*, 1301-1308. https://doi.org/10.1016/S0045-6535(02)00530-1

Meza-Montenegro, M.M., Gandolfi, A.J., Santana-Alcántar, M.E., Klimecki, W.T., Aquilar-Apodaca, M.G., Del Río-Salas, R., De la O-Villanueva, M., Gómez-Alvarez, A., Mendivil-Quijada, H., & Valencia, M. (2012). Metals in residential soils and cumulative risk assessment in Yaqui and Mayo agricultural valleys, northern Mexico. *Sci. Total Environ*, *433*, 472-481. https://doi.org/10.1016/j.scitotenv.2012.06.083

Matta, C.F., Ayers, P.W. & Cook, R. (2024). The Physics of electron localization and delocalization. In *Electron Localization-Delocalization Matrices*, 7-20. Springer International Publishing. https://doi.org/10.1007/978-3-031-51434-0_2

Mishra, N.S., Saravanan, P. (2018). A review on the synergistic features of hexagonal boron nitride (white graphene) as adsorbent-photo active nanomaterial. *ChemistrySelect*, *3*(28), 8023-8034. https://doi.org/10.1002/slct.201801524

Mollaamin, F., Monajjemi, M. (2023). Transition metal (X = Mn, Fe, Co, Ni, Cu, Zn)-doped graphene as gas sensor for CO2 and NO2 detection: a molecular modeling framework by DFT perspective. *J. Mol. Model, 29*, 119. https://doi.org/10.1007/s00894-023-05526-3

Mollaamin, F. (2024). Competitive Intracellular Hydrogen-Nanocarrier Among Aluminum, Carbon, or Silicon Implantation: a Novel Technology of Eco-Friendly Energy Storage using Research Density Functional Theory. *Russ. J. Phys. Chem. B., 18*, 805–820. https://doi.org/10.1134/S1990793124700131

Mollaamin, F., Monajjemi, M. (2024a). The influence of Sc, V, Cr, Co, Cu, Zn as ferromagnetic semiconductors implanted on B_5N_{10}-nanocarrier for enhancing of NO sensing: An environmental eco-friendly investigation. *Computational and Theoretical Chemistry*, *1237*, 114666. https://doi.org/10.1016/j.comptc.2024.114666

Mollaamin, F., Monajjemi, M. (2024b). Boron nitride doped with transition metals for carbon monoxide detection: a promising nanosensor for air cleaning. *Sensor Review*, *44*(2), 179-193. https://doi.org/10.1108/SR-01-2024-0066

Mollaamin, F., Monajjemi, M. (2024c). Effect of Implanted Titanium, Vanadium or Chromium on Boron Nitride Surface for Increasing Carbon Monoxide Adsorption: Designing Gas Sensor for Green Chemistry Future. *Russ. J. Phys. Chem. B., 18*, 1199-1216. https://doi.org/10.1134/S1990793124700519

Mollaamin, F., Monajjemi, M. (2024d). Selectivity and Sensitivity Evaluation of Embedded BN-Nanostructure as a Gas Detector for Air Pollution Scavenging: a Theoretical Study. *Russ. J. Phys. Chem. B.*, *18*, 1177-1198. https://doi.org/10.1134/S1990793124700507

Mollaamin, F., Monajjemi, M. (2024e). Designing novel nanomaterials for Li-ion batteries: A physico-chemical study through hydrogen-powered horizons. *New Materials, Compounds and Applications, 8*(3), 303-323. https://doi.org/10.62476/nmca83303

Mollaamin, F., Mohammadi, S., Khalaj, Z., & Monajjemi, M. (2024). Computational Modelling of Boron Nitride Nanosheet for Detecting and Trapping of Water Contaminant. *Russ. J. Phys. Chem. B., 18*, 67-82. https://doi.org/10.1134/S1990793124010330

Montagne, D., Cornu, S., Bourennane, H.N., Baize, D., Ratié, C., King, D. (2007). Effect of agricultural practices on trace-element distribution in soil. *Commun. Soil Sci. Plant Anal.*, *38*, 473-491. https://doi.org/10.1080/00103620601174411

Morton-Bermea, O., Hernández-Alvarez, E., González-Hernández, G., Romero, F., Lozano, R., & Beramendi-Orosco, L.E. (2009). Assessment of heavy metal pollution in urban topsoils from the metropolitan area of Mexico City. *J. Geochem. Explor.*, *101*, 218-224. https://doi.org/10.1016/j.gexplo.2008.07.002

Motuzova, G.V., Minkina, T.M., Karpova, E.A., Barsova, N.U., & Mandzhieva, S.S. (2014). Soil contamination with heavy metals as a potential and real risk to the environment, *Journal of Geochemical Exploration*, *144*, Part B, 241-246. https://doi.org/10.1016/j.gexplo.2014.01.026

O'boyle, N.M., Tenderholt, A.L. & Langner, K.M. (2008). Cclib: A library for package?independent computational chemistry algorithms. *Journal of Computational Chemistry*, *29*(5), 839-845. https://doi.org/10.1002/jcc.20823

Onawumi, O.O., Olaniyan, J.A., Esan,A.O., Adewusi, O.A., Yusuff, A.O., & Odedele, A.O. (2024). *Materials International*, *6*(3), 27. https://doi.org/10.33263/Materials63.027

Perdew, J.P., Burke, K. & Ernzerhof, M. (1996). Generalized gradient approximation made simple. *Physical Review Letters*, *77*(18), 3865. https://doi.org/10.1103/PhysRevLett.77.3865

Poggere, G., Gasparin, A., Barbosa, J.Z., Melo, G.W., Corrêa, R.S., & Motta, A.C.V. (2023). Soil contamination by copper: Sources, ecological risks, and mitigation strategies in Brazil. *Journal of Trace Elements and Minerals*, *4*, 100059. https://doi.org/10.1016/j.jtemin.2023.100059

Rahman, S.H., Khanam, D., Adyel, T.M., Islam, M.S., Ahsan, M.A., & Akbor, M.A.(2012). Assessment of Heavy Metal Contamination of Agricultural Soil around Dhaka Export Processing Zone (DEPZ), Bangladesh: Implication of Seasonal Variation and Indices. *Appl. Sci. 2*, 584-601. https://doi.org/10.3390/app2030584

Sarasia, E.M., Afsharnezhad, S., Honarparvar, B., Mollaamin, F., & Monajjemi, M. (2011). Theoretical study of solvent effect on NMR shielding tensors of luciferin derivatives. *Physics and Chemistry of Liquids*, *49*(5), 561-571. https://doi.org/10.1080/00319101003698992

Savin, A., Jepsen, O., Flad, J., Andersen, O.K., Preuss, H. & von Schnering, H.G. (1992). Electron localization in solid?state structures of the elements: The diamond structure. *Angewandte Chemie International Edition in English*, *31*(2), 187-188. https://doi.org/10.1002/anie.199201871

Sezgin, N., Ozcan, H.K., Demir, G., Nemlioglu, S., & Bayat, C. (2003). Determination of heavy metal concentrations in street dusts in Istanbul E-5 highway. *Environ. Int.*, *29*, 979-985. https://doi.org/10.1016/S0160-4120(03)00075-8

Shtansky, D.V., Matveev, A.T., Permyakova, E.S., Leybo, D.V., Konopatsky, A.S., & Sorokin, P.B. (2022). Recent Progress in Fabrication and Application of BN Nanostructures and BN-Based Nanohybrids. *Nanomaterials*, *12*, 2810. https://doi.org/10.3390/nano12162810

Stephens, P.J., Devlin, F.J., Chabalowski, C.F. & Frisch, M.J. (1994). Ab initio calculation of vibrational absorption and circular dichroism spectra using density functional force fields. *The Journal of Physical Chemistry*, *98*(45), 11623-11627. https://doi.org/10.1021/j100096a001

Sun, G.Y., Chen, Y.P., Bi, X.Y., Yang, W., Chen, X.S., Zhang, B., & Cui, Y.J. (2013). Geochemical assessment of agricultural soil: A case study in Songnen-Plain (Northeastern China). *Catena*, *111*, 56-63. https://doi.org/10.1016/j.catena.2013.06.026

Sun, G.Y., Li, Z.G., Bi, X.Y., Chen, Y.P., Lu, S.F., & Yuan, X. (2013). Distribution, sources and health risk assessment of mercury in kindergarten dust. *Atmos. Environ*, *73*, 169-176. https://doi.org/10.1016/j.atmosenv.2013.03.017

Tahan, A., Mollaamin, F. & Monajjemi, M. (2009). Thermochemistry and NBO analysis of peptide bond: Investigation of basis sets and binding energy. *Russ. J. Phys. Chem.*, *83*, 587-597. https://doi.org/10.1134/S003602440904013X

Thuy, H., Tobschall, H. & An, P. (2000). Distribution of heavy metals in urban soils – a case study of Danang-Hoian Area (Vietnam). *Environmental Geology, 39*, 603-610. https://doi.org/10.1007/s002540050472

Vosko, S.H., Wilk, L. & Nusair, M. (1980). Accurate spin-dependent electron liquid correlation energies for local spin density calculations: A critical analysis. *Canadian Journal of Physics*, *58*(8), 1200-1211. https://doi.org/10.1139/p80-159

Weng, Q.H., Wang, X.B., Wang, X., Bando, Y., & Golberg, D. (2016). Functionalized hexagonal boron nitride nanomaterials: emerging properties and applications. *Chem. Soc. Rev.*, *45*(14), 3989-4012. https://doi.org/10.1039/C5CS00869G

Yanai, T., Tew, D.P. & Handy, N.C. (2004). A new hybrid exchange-correlation functional using the Coulomb-attenuating method (CAM-B3LYP). *Chemical Physics Letters*, *393*(1-3), 51-57. https://doi.org/10.1016/j.cplett.2004.06.011

Zadeh, M.A.A., Lari, H., Kharghanian, L., Balali, E., Khadivi, R., Yahyaei,H. Mollaamin, F., & Monajjemi, M.(2015). Density Functional Theory Study and Anti-Cancer Properties of Shyshaq Plant: In View Point of Nano Biotechnology. *J Comput Theor Nanosci*, *12*(11), 4358–4367. https://doi.org/10.1166/jctn.2015.4366

Ziesche, P., Kurth, S. & Perdew, J.P. (1998). Density functionals from LDA to GGA. *Computational Materials Science*, *11*(2), 122-127. https://doi.org/10.1016/S0927-0256(97)00206-1